JAEA-Data/Code
2018-009
DOI:10.11484/jaea-data-code-2018-009

JAEA-Data/Code

Error Estimation in Observed Acceleration Data toward V&V of a Seismic Simulation

Yoshio SUZUKI and Kazuhiko IIGAKI

Center for Computational Science & e-Systems

September 2018

Japan Atomic Energy Agency

日本原子力研究開発機構

本レポートは国立研究開発法人日本原子力研究開発機構が不定期に発行する成果報告書です。
本レポートの入手並びに著作権利用に関するお問い合わせは、下記あてにお問い合わせ下さい。
なお、本レポートの全文は日本原子力研究開発機構ホームページ（http://www.jaea.go.jp）
より発信されています。

国立研究開発法人日本原子力研究開発機構 研究連携成果展開部 研究成果管理課
〒319-1195 茨城県那珂郡東海村大字白方 2 番地4
電話 029-282-6387, Fax 029-282-5920, E-mail:ird-support@jaea.go.jp

This report is issued irregularly by Japan Atomic Energy Agency.
Inquiries about availability and/or copyright of this report should be addressed to
Institutional Repository Section,
Intellectual Resources Management and R&D Collaboration Department,
Japan Atomic Energy Agency.
2-4 Shirakata, Tokai-mura, Naka-gun, Ibaraki-ken 319-1195 Japan
Tel +81-29-282-6387, Fax +81-29-282-5920, E-mail:ird-support@jaea.go.jp

JAEA-Data/Code 2018-009

Error Estimation in Observed Acceleration Data toward V&V of a Seismic Simulation

Yoshio SUZUKI and Kazuhiko IIGAKI+

Center for Computational Science & e-Systems
Japan Atomic Energy Agency
Kashiwa-shi, Chiba-ken

(Received May 28, 2018)

Toward Verification & Validation (V&V) of a seismic simulation of entire nuclear plant, an approach to estimate errors included in observed acceleration data is proposed. On the comparison between simulation results and experimental or observational results in the process of V&V, errors which might be included in experimental or observational data should be estimated. It is considered that there exist following two causes for errors in observed acceleration data; measurement accuracy of an accelerometer measurement system and disturbance included in measured data. Techniques based on the specification of an accelerometer measurement system and the time series analysis are respectively adopted to estimate those errors. To clarify the actual procedure, those techniques are applied to acceleration data observed at High Temperature engineering Test Reactor (HTTR) at the Oarai Research and Development Institute of Japan Atomic Energy Agency. Firstly, to estimate errors caused by measurement accuracy, errors for the anti-aliasing filter in the recording equipment and the seismometer property are calculated. Here, the low-pass filter to evaluate the frequency range of interest is also used. In addition, errors caused by the transverse sensitivity and the linearity are calculated. Secondly, to estimate errors caused by disturbance, two time series analysis models (the autoregressive (AR) model and the locally stationary AR (LSAR) model) are used. As a result of error estimation, it is found that for acceleration data used in this research the absolute value of error of maximum amplitude is under about 6%.

Keywords: V&V, Error Estimation, Seismic Analysis, Accelerometer Measurement System

+ Department of HTTR, HTGR Research and Development Center, Oarai Research and Development Institute, Sector of Fast Reactor and Advanced Reactor Research and Development

JAEA-Data/Code 2018-009

耐震シミュレーションの検証・妥当性確認に向けた観測された加速度データの誤差推定

日本原子力研究開発機構　システム計算科学センター

鈴木　喜雄、飯垣　和彦+

(2018 年 5 月 28 日　受理)

原子力施設全体を対象とした耐震シミュレーションの検証・妥当性確認（V&V）に向け、観測により得られた加速度データに含まれる誤差を推定するためのアプローチを提案する。V&V のプロセスにおいて、シミュレーション結果と実験/観測結果を比較するには、実験/観測データに含まれる誤差を推定する必要がある。観測された加速度データには、観測システム自身が有する計測精度に関わる誤差と、観測システムが計測したデータに含まれ得る外乱から生じる誤差の二つがあると考えた。これらの誤差を推定するため、加速度計測システムの仕様に基づく手法と、時系列解析手法をそれぞれ用いることとした。また、実際の手順を明確にするため、これらの手法を日本原子力研究開発機構大洗研究所の高温工学試験研究炉（HTTR）で観測された加速度データに適用している。まず、計測精度に関わる誤差を推定するため、集録装置におけるアンチエイリアスフィルタと、感震器特性に対する誤差を算出している。ここで、対象とする周波数範囲の評価のためローパスフィルタも用いている。また、横感度および直線性に起因する誤差を算出している。次に、外乱に起因する誤差を推定するため、2 種類の時系列解析モデル（自己回帰（AR）モデルと局所定常自己回帰（LSAR）モデル）を用いている。誤差推定の結果、今回用いた加速度データに対しては、最大振幅の誤差の絶対値は約 6%以下になることが分かった。

システム計算科学センター（駐在）：〒277-0871 千葉県柏市若柴 178-4 柏の葉キャンパス 148 街区 4

＋　高速炉・新型炉研究開発部門大洗研究所高温ガス炉研究開発センター高温工学試験研究炉部

Contents

目　次

表リスト

図リスト

1. Introduction

Our objective is to propose an approach to estimate errors included in acceleration data observed at nuclear facilities toward Verification & Validation (V&V)[1,2] of a seismic simulation of entire nuclear plant[3]. In the process of V&V, a conceptual model is constructed with idealizing a reality of interest, and a mathematical modeling and a physical modeling are performed for the conceptual model (Fig. 1). Simulation results and experimental or observational results are obtained with the mathematical modeling and the physical modeling, respectively. The credibility of simulation is evaluated by comparing simulation results with experimental or observational results. To evaluate it, errors in simulation results and experimental or observational results (δ_s and δ_D) are estimated and their uncertainties are derived. The conceptual model must be common to estimate those errors.

We consider the use of acceleration data observed at a facility not only as observational results to compare simulation results but also as input data in the simulation. Then, it is appropriate to regard an "ideal seismic acceleration" loading on the facility as input data in the conceptual model (Fig. 1). By using the "ideal seismic acceleration" as input data of the seismic simulation, ideal "simulation results" based on the conceptual model are obtained. And the acceleration caused when the "ideal seismic acceleration" loads on the facility is regarded as ideal "observational results" based on the conceptual model. Those ideal simulation results and ideal observational results should be used for the comparison. Since the ideal seismic acceleration and the ideal observational results cannot be obtained, however, it is needed to estimate them. These ideal values should be represented with error ranges in which the real value would be included. One essential issue is how to estimate those errors.

As an approach to estimate those errors, it is considered that those errors are represented by errors which could be included in the observed value and that the ideal values are represented by the observed value and such errors by expecting the observed value is close to the real value. Then, the estimation of ideal values is equivalent to the estimation of those errors. As shown in Fig. 1, the observed acceleration is obtained by measuring with an observational system (accelerometer measurement system) the acceleration which is caused when the ideal seismic acceleration with disturbance loads on the system. Therefore, it is considered that there exist following two causes for errors: one is disturbance which is included in data measured by an observational system and the other is measurement accuracy which is included in the observational system.

To estimate those errors, factors consisting of those causes of errors are examined and methods to estimate errors caused by those factors are investigated in existing researches. As a result, we could hardly find any cases in which those factors were individually evaluated and errors were estimated. On the other hand, we found some cases in which components regarded as errors were estimated using various filters and/or the time series

analysis. Exploiting methods to estimate components regarded as errors in existing researches, an approach to estimate errors is proposed. Firstly, errors which are caused by measurement accuracy included in an observational system are estimated using techniques individually suitable to specification items of an observational system. Secondly, errors which are caused by disturbance included in data measured by an observational system are estimated using the time series analysis. Here, it is important to consider the sequence of error estimations. Those results are shown in section 2. To clarify the actual procedure of proposed approach, this approach is applied to acceleration data observed at High Temperature engineering Test Reactor (HTTR)[4] located at Oarai Research and Development Institute of the Japan Atomic Energy Agency. The results are shown in section 3. Finally, in section 4 we summarize our results.

2. Approach for error estimation

2.1 Examination of error factors

As indicated in section 1, two causes of errors are considered: disturbance which is included in data measured by an observational system and measurement accuracy which is included in the observational system. We examine factors for each cause. Especially references 5), 6) and 7) are useful. The result is as follows.

2.1.1 Errors caused by disturbance which is included in data measured by an observational system

Factors for errors caused by disturbance are considered to be as follows.

· mechanical vibration

· microtremor

The mechanical vibration is caused when machines in a facility are working and affects the vibration of facility. Since such a mechanical vibration is not considered in our seismic simulation, the mechanical vibration should not be included in the “ideal seismic acceleration”. On the other hand, since the mechanical vibration could be included in the “observed acceleration”, it should be treated as a factor caused by disturbance.

Acceleration data of the microtremor cannot be exactly obtained, so that it cannot be included in input data of the simulation, namely the “ideal seismic acceleration”. Thus, we treat the microtremor as disturbance.

2.1.2 Errors caused by measurement accuracy which is included in an observational system

Keeping the observational system used in HTTR in mind, we focus on an observational system consisting of three components: a seismometer, a transmission equipment, and a recording equipment. Error factors for each component are considered to be as follows.

(1) seismometer
· offset
· gain
· linearity
· responsibility
· monotonicity
· repeatability
· temperature characteristics
· transverse sensitivity
· resolution
· property (amplitude property and phase property)

(2) transmission equipment
· transmission

(3) recording equipment
· filter
· quantization

The filter in recording equipment is mainly an anti-aliasing filter to suppress the generation of aliasing. The low-pass filter is used as the anti-aliasing filter to cut frequency being more than half of the sampling frequency.

The installation and the aging degradation are enumerated as error factors except those mentioned above. Those factors are not considered in this paper. How to treat those factors is a future issue. Acceleration data used in section 3, however, are ones after azimuth correction.

2.2 Error estimation method in existing researches

We investigated a method to estimate errors included in acceleration data in existing researches. In the investigation, we intended for 139 documents for the past five years in the structure engineering field and earthquake engineering field where the description about acceleration data was frequent[8]. However, we could hardly find any cases in which error factors were individually evaluated and errors were estimated. In a lot of documents (about 70%), observed data are just used without estimating errors. In the remaining ones, observed data which are corrected with a process that components regarded as errors are removed are used. The low-pass filter, the high-pass filter, the reverse filter, and/or the time series analysis are used for the process. The low-pass filter is mainly used to remove higher frequency range than the frequency of interest. The high-pass filter is mainly used to reduce

errors when displacements are derived from accelerations with integration. The reverse filter is used to reduce errors of frequency range in which the reception reduces by using the anti-alias filter. The time series analysis is used to remove errors in a lump whose independent estimation is difficult. Various models of the time series analysis and its application examples are indicated in references 9), 10) and 11). For example, the autoregressive (AR) model is applied to catch the change of observed data of a bridge vibration when damage occurred to the bridge, and the local stationary autoregressive (LSAR) model is applied to extract a characteristic wave pattern from observed data of an earthquake vibration.

Our objective is to estimate errors of observed acceleration data toward V&V of a seismic simulation for entire nuclear facility. To achieve this, it is considered to be important to evaluate each error factor examined in section 2.1 as well as to estimate those errors individually and integrally. We apply appropriate error estimation techniques to error factors and finally estimate errors integrally. We use some of techniques to remove errors indicated in existing researches.

2.3 Proposed approach

As shown in section 1, errors caused by disturbance which is included in data measured by an observational system (“disturbance acceleration”) are added to the “ideal seismic acceleration”, and errors caused by measurement accuracy in an observational system are further added to the acceleration that the “ideal seismic acceleration” plus the “disturbance acceleration”. We estimate the “ideal seismic acceleration” by following a reverse process. Namely, errors caused by measurement accuracy are firstly estimated to derive the acceleration that the “ideal seismic acceleration” plus the “disturbance acceleration”. The “disturbance acceleration” is secondly estimated to derive the “ideal seismic acceleration”.

2.3.1 Estimation of errors caused by measurement accuracy which is included in an observational system

Checking error factors examined in section 2.1 with specification items of an observational system, appropriate techniques to estimate errors are adopted. Here, the sequence in which errors are caused should be considered. Namely, errors in a recording equipment, a transmission equipment, and a seismometer are estimated in this order.

Comparing magnitudes of errors, error factors with smaller ones are assumed to be negligible. There are also some factors whose necessity is judged depending on the acceleration frequency of interest. The relation between the cutoff frequency of the anti-aliasing filter in the recording equipment and the eigen frequency of parts/equipments in a nuclear facility is essential. For example, there is a case that about 30Hz is set as the cutoff frequency in a nuclear facility. This is because to cut the frequency range more than 50Hz

for the sampling frequency 100Hz. On the other hand, the range of eigen frequency of parts/equipments in a nuclear facility is about 1Hz to 40Hz. Thus, errors are caused for both the amplitude modulation and the phase modulation of acceleration data the anti-aliasing filter generates. The relation between seismometer property and the eigen frequency of parts/equipments in a nuclear facility is also important because of the same reason.

The cutoff frequency of the anti-aliasing filter in the observational system in HTTR, to which our proposed approach is applied, is 30.5Hz[12] and thus the reception gradually reduces from about 20Hz. In addition, there exist parts/equipments with 38Hz eigen frequency[13]. Therefore, errors for both the amplitude and the phase of acceleration can be generated in the frequency range where the reception reduces.

2.3.2 Estimation of errors caused by disturbance which is included in data measured by an observational system

To estimate errors caused by disturbance (which is the same as the "disturbance acceleration"), we use the time series analysis since it is difficult to quantitatively estimate errors caused by disturbance using such means used to estimate errors caused by measurement accuracy. We use the autoregressive (AR) model[9] and the locally stationary AR (LSAR) model[9], which are basic models of the time series analysis.

3. Application of the proposed approach to acceleration data observed in HTTR

3.1 Target seismic motion

Seven seismic motions, whose magnitude at the epicenter is more than 5.0, shown in Table 1 are used in the seismic simulation of HTTR[14]. In this paper, the last four motions are used. In section 3.3 and 3.4, acceleration data in the north-south (NS) direction observed at the center of B3 floor in the HTTR building for the wave No. 4 is used. Data observed at the center of B3 floor are used as input data in the seismic simulation of HTTR[14] since the floor is close to the ground. In section 3.5, acceleration data in the NS direction observed at the center of B3 floor, the south side of 1st floor, and the south side of 2nd floor for waves No. 4, 6 and 7 are used. Used observed points are shown in Fig.2. In section 3.6, acceleration data in the NS direction for waves No.4, 5, 6 and 7 are used. The acceleration data used is cut out for 40.96 second. The time step is 0.01 second. Thus, the number of data is 4096.

3.2 Specification of observational system installed in HTTR

Specification items of the observational system installed in HTTR is shown in Table 2[8,13]. In HTTR, accelerometers are installed in the ground and the building[13]. We focus on accelerometers in the building. Some of their data are used as input data in the simulation.

3.3 Estimation of errors caused by measurement accuracy

3.3.1 Assumption of error factors

We assume errors as follows by checking error factors in section 2.1 with specification items of the observational system in section 3.2.

(1) Seismometer

· offset	negligible
· gain	negligible
· linearity	±0.66[cm/s^2]
· responsibility	negligible
· monotonicity	negligible
· repeatability	negligible
· temperature characteristics	negligible
· transverse sensitivity	±0.008×sum of amplitudes in other two directions [cm/s^2]
· resolution	negligible
· property	eigen frequency 150[Hz], amplitude error and phase error derived from the damping ratio 0.7

(2) Transmission equipment

· transmission	negligible

(3) Recording equipment

· filter	error caused by anti-aliasing filter (cutoff frequency 30.5Hz, slope -24db/Oct, Butterworth characteristics)
· quantization	negligible

For the error caused by the linearity, the corresponding voltage is derived from the maximum voltage (11[V]×0.0003 = 3.3[mV]) and is converted to the acceleration (3.3[mV]/5[mV/cm/s^2] = 0.66[cm/s^2]). Shown in Table 2, the linearity of seismometer is smaller than that of transmission equipment, so only the linearity of transmission equipment is adopted. The error caused by the resolution becomes ±0.001[cm/s^2]. The maximum error caused by the temperature characteristics is obtained from the amplitude multiplied by 0.0006 when the temperature change during measurement is assumed to be equal to or less than one degree. For the error caused by the quantization, the corresponding voltage is derived from the value of A/D conversion$(20/(20^{16}-1)/\sqrt{12} \approx 0.09[\mathrm{mV}])$[15] and is converted to the acceleration (0.09[mV]/5[mV/cm/s^2] = 0.018[cm/s^2]). Errors caused by the

resolution, the temperature characteristics, the quantization, and other factors assumed to be negligible are less than ones caused by the linearity and the transverse sensitivity.

3.3.2 Error estimation

Under the assumption in section 3.3.1, we estimate the acceleration that the "ideal seismic acceleration" plus the "disturbance acceleration". Firstly, we estimate errors caused by the anti-aliasing filter in the recording equipment and the seismometer property. In addition, we use the low-pass filter to estimate the frequency range off interest.

① Reverse filter to estimate errors caused by the anti-aliasing filter

We use the reverse filter for 4th order Butterworth filter as shown in Eq. (1) to (3) to estimate the amplitude error and the phase error caused by the anti-aliasing filter.

$$F_1(f) = 1/\left(A_1(f)e^{i\phi_1(f)}\right) \quad (1)$$

$$A_1(f) = 1/\sqrt{1+(f/f_c)^8} \quad (2)$$

$$\phi_1 = \tan^{-1}\left(\frac{2.613((f/f_c)^3 - f/f_c)}{(f/f_c)^4 - 3.414(f/f_c)^2 + 1}\right) \quad (3)$$

Here, f is the frequency and $f_c = 30.5$ based on the specification.

② Reverse filter to estimate errors caused by the seismometer property

We use the reverse filter shown in Eq. (4) to (6) to estimate the amplitude error and the phase error caused by the seismometer property (for ex. see the reference 16)).

$$F_2(f) = 1/\left(A_2(f)e^{i\phi_2(f)}\right) \quad (4)$$

$$A_2(f) = 1/\sqrt{(1-(f/f_s)^2)^2 + \left(2h_s(f/f_s)\right)^2} \quad (5)$$

$$\phi_2 = -\tan^{-1}\left(\frac{2h_s(f/f_s)}{1-(f/f_s)^2}\right) \quad (6)$$

Here, $f_s = 150.0$, $h_s = 0.7$ based on the specification.

③ Low-pass filter to estimate the frequency range off interest

We focus on the frequency range less than 50Hz so that we use the filter shown in Eq. (7).

$$F_3(f) = A_3(f) = \begin{cases} 1 & 0 \le f \le f_{ul} \\ \frac{f_{uu}-f}{f_{uu}-f_{ul}} & f_{ul} \le f \le f_{uu} \end{cases} \quad (7)$$

This filter is the same used in the reference 16). Here, we use $f_{ul} = 30.5$, $f_{uu} = 50.0$. As the combination of those three filters, we can get the filter shown in Eq. (8) to (10).

$$F_s(f) = 1/\left(A(f)e^{i\emptyset(f)}\right) \quad (8)$$

where

$$A(f) = A_1(f) \cdot A_2(f)/A_3(f) \quad (9)$$

$$\emptyset(f) = \emptyset_1(f) + \emptyset_2(f) \quad (10)$$

Graphs of Eq. (2), (5), (7) and (9), and Eq. (3), (6), and (10) are shown in Fig. 3 (a) and (b), respectively.

The original data (observed data) are shown in Fig. 4. And the estimated acceleration data obtained by applying $F_1(f)$, $F_2(f)$ and $F_3(f)$ in which errors are estimated using Eq. (8) are shown in Fig. 5. The acceleration data is firstly Fourier-transformed, and then, inverse Fourie-transformed after applying $F_1(f)$, $F_2(f)$ and $F_3(f)$. The peak that an absolute value of amplitude becomes the maximum value in the observed data is 30.64[cm/s^2] at 8.62[s]. The peak in the estimated acceleration data is 30.38[cm/s^2] at 8.61[s]. Then, the difference of maximum amplitude is 0.85%. That after applying $F_1(f)$ is 0.61%, and that after applying $F_1(f)$ and $F_2(f)$ is 1.18%. Thus, the suppression of the use of $F_3(f)$ is about 0.33%. To confirm how much that suppression is reduced for larger f_{ul} in $F_3(f)$, $f_{ul} = 45.0$, as one example, is used. In this case, the difference of maximum amplitude becomes 0.88%. The influence for difference of f_{ul} is small.

Secondly, we estimate errors caused by the transverse sensitivity and the linearity.

④ Process to estimate errors caused by the transverse sensitivity

To estimate errors caused by the transverse sensitivity, the following process is performed using the estimated acceleration data in east-west (EW) and up-down (UD) directions after applying $F_1(f)$, $F_2(f)$ and $F_3(f)$. NS, EW and UD directions are orthogonal to each other.

$$F_{4\pm}(t) = \pm 0.008 A_{sum}(t) \quad (11)$$

Namely, $F_{4\pm}(t)$ is added to the acceleration data in NS direction after Fourier-transformation, application of $F_s(f)$, and inverse Fourier-transformation. Here, t is the time and $A_{sum}(t)$ means time series of sum of accelerations in other two directions, namely, sum of accelerations in EW and UD direction after Fourier-transformation, application of $F_s(f)$, and inverse Fourier-transformation.

⑤ Process to estimate errors caused by the linearity

To estimate errors caused by the linearity, ±0.66[cm/s^2] are added by the acceleration data after adding $F_{4\pm}(t)$.

$$F_{5\pm}(t) = \pm 0.66 \quad (12)$$

Errors from $F_{4-}(t)$ and $F_{5+}(t)$ are shown in Fig. 6 (a). The combination of $F_{4-}(t)$ and $F_{5+}(t)$ and the combination of $F_{4-}(t)$ and $F_{5-}(t)$ are shown in Fig. 6 (b). $F_{4-}(t)$ is plotted by the broken line near zero. $F_{5+}(t)$ are plotted by dotted lines. Errors caused by the linearity are larger than those caused by the transverse sensitivity. The acceleration data in which errors are estimated considering processes ①, ②, ③, ④(-) and ⑤(±) are shown in Fig. 7 (a) and (b). In these figures, $F_1(f)$, $F_2(f)$, $F_3(f)$, $F_{4-}(t)$ and $F_{5\pm}(t)$ are applied to the observed data. These data are the estimated acceleration data for the ideal seismic acceleration plus the disturbance acceleration. The difference of maximum amplitude before and after applying $F_1(f)$, $F_2(f)$, $F_3(f)$, $F_{4-}(t)$ and $F_{5+}(t)$ is 1.36%. That before and after applying $F_1(f)$, $F_2(f)$, $F_3(f)$, $F_{4-}(t)$ and $F_{5-}(t)$ is 2.95%.

Errors from $F_{4+}(t)$ and $F_{5+}(t)$ are shown in Fig. 8 (a). The combination of $F_{4+}(t)$ and $F_{5+}(t)$ and the combination of $F_{4+}(t)$ and $F_{5-}(t)$ are shown in Fig. 8 (b). $F_{4+}(t)$ is plotted by the broken line near zero. $F_{5+}(t)$ are plotted by dotted lines. The acceleration data in which errors are estimated considering processes ①, ②, ③, ④(+) and ⑤(±) are shown in Fig. 9 (a) and (b). In these figures, $F_1(f)$, $F_2(f)$, $F_3(f)$, $F_{4+}(t)$ and $F_{5\pm}(t)$ are applied to the observed data. The difference of maximum amplitude before and after applying $F_1(f)$, $F_2(f)$, $F_3(f)$, $F_{4+}(t)$ and $F_{5+}(t)$ are 1.25%. That before and after applying $F_1(f)$, $F_2(f)$, $F_3(f)$, $F_{4+}(t)$ and $F_{5-}(t)$ is 3.06%.

Therefore, the maximum and minimum differences of maximum amplitude before and after applying ① to ⑤ processes are 3.06% and 1.25%, respectively. The differences are summarized in Table 3.

Figures 10 and 11 (a) show Fourier spectrums of the observed acceleration data, and of

the estimated acceleration data by applying $F_1(f)$, $F_2(f)$ and $F_3(f)$, respectively. Figure 11 (b) shows the absolute value of difference of Fourier spectrums before and after applying $F_1(f)$, $F_2(f)$ and $F_3(f)$. From Fig. 11 (b), Fourier spectrum with higher frequency range becomes larger by applying $F_1(f)$, $F_2(f)$ and $F_3(f)$.

Figure 12 (a) and (b) show Fourier spectrum of the estimated acceleration data by applying $F_1(f)$, $F_2(f)$, $F_3(f)$, $F_{4-}(t)$ and $F_{5+}(t)$, and the absolute value of difference of Fourier spectrums before and after applying $F_{4-}(t)$ and $F_{5+}(t)$, respectively. From Fig. 12 (b), Fourier spectrum with lower frequency range become larger by applying $F_{4-}(t)$ and $F_{5+}(t)$. Figure 13 (a) and (b) show Fourier spectrum of the estimated acceleration data by applying $F_1(f)$, $F_2(f)$, $F_3(f)$, $F_{4-}(t)$ and $F_{5-}(t)$, and the absolute value of difference of Fourier spectrums before and after applying $F_{4-}(t)$ and $F_{5-}(t)$, respectively. Figure 14 (a) and (b) show Fourier spectrum of the estimated acceleration data by applying $F_1(f)$, $F_2(f)$, $F_3(f)$, $F_{4+}(t)$ and $F_{5+}(t)$, and the absolute value of difference of Fourier spectrums before and after applying $F_{4+}(t)$ and $F_{5+}(t)$, respectively. Figure 15 (a) and (b) show Fourier spectrum of the estimated acceleration data by applying $F_1(f)$, $F_2(f)$, $F_3(f)$, $F_{4+}(t)$ and $F_{5-}(t)$, and the absolute value of difference of Fourier spectrums before and after applying $F_{4+}(t)$ and $F_{5-}(t)$, respectively. The difference between results by applying $F_{5+}(t)$ and $F_{5-}(t)$ (Fig.12 and Fig.13, or Fig.14 and Fig.15) occurs only at $f = 0$ because $F_{5\pm}(t)$ is constant. The difference between results by applying $F_{4+}(t)$ and $F_{4-}(t)$ is small because the absolute value of $F_{4\pm}(t)$ is smaller.

3.4 Estimation of errors caused by disturbance

3.4.1 Error estimation

Here, the autoregressive (AR) model and the locally stationary AR (LSAR) model are applied to the acceleration data after estimation in section 3.3.

⑥-1 Process to estimate errors caused by disturbance using the AR model

The AR model, when time series $y_1, \cdots, y_N$ are given, is represented by Eq. (13).

$$y_n = \sum_{i=1}^{m} a_i y_{n-i} + v_n \qquad (13)$$

Here, n is given by $1, \cdots, N$ where N is the number of data (thus, $N = 4096$ in our case). a_i is the autoregression coefficient. v_n corresponds to the residual that is a part which cannot be explained from the variation of y_{n-i} and represents the white noise with average zero and dispersion σ^2. The standard deviation σ of white noise is regarded as errors caused

by disturbance. m is the degree of autoregression. Defining $\theta = (a_1, \cdots, a_m, \sigma^2)$ and Solving θ to maximize the log likelihood $l(\theta) = \sum_{n=1}^{N} \log p(y_n | y_1, \cdots, y_{n-1}, \theta)$, θ is determined. Here, the Yule-Walker method[9], which is generally used as one of methods to solve that, is used. Then, solving m to minimize the Akaike Information Criterion (AIC)[9] ($\mathrm{AIC}_m = N(\log 2\pi\sigma_m^2 + 1) + 2(m+1)$), m is determined. In our case m becomes 200 ($m = 200$ for $n > 200$, but $m = n - 1$ for $n \leq 200$). Using the acceleration data after applying $F_1(f)$, $F_2(f)$, $F_3(f)$, $F_{4\pm}(t)$ and $F_{5\pm}(t)$ for $y_1, \cdots, y_N$, errors caused by disturbance is estimated.

Figure 16 (a) and (b) show standard deviations $\pm\sigma$ when substituting the acceleration data after applying $F_1(f)$, $F_2(f)$, $F_3(f)$, $F_{4-}(t)$ and $F_{5\pm}(t)$. The standard deviations in those cases are the same. The solid line and the dotted line are used for $+\sigma$ and $-\sigma$, respectively. Symbols ⑥-1 is used for the process by the AR model. Figure 17 (a) and (b) show accelerations estimated by AR model for the acceleration obtained by applying $F_1(f)$, $F_2(f)$, $F_3(f)$, $F_{4-}(t)$ and $F_{5+}(t)$, and by applying $F_1(f)$, $F_2(f)$, $F_3(f)$, $F_{4-}(t)$ and $F_{5-}(t)$, respectively. The difference of maximum amplitudes before and after applying $F_1(f)$, $F_2(f)$, $F_3(f)$, $F_{4-}(t)$, $F_{5+}(t)$ and the AR model is 2.44%. That before and after applying $F_1(f)$, $F_2(f)$, $F_3(f)$, $F_{4-}(t)$, $F_{5-}(t)$ and the AR model is 1.48%. The difference between cases with $F_{5+}(t)$ and $F_{5-}(t)$ is caused by the difference of the autoregression coefficient a_i.

Figure 18 (a) and (b) show standard deviations $\pm\sigma$ when substituting the acceleration data after applying $F_1(f)$, $F_2(f)$, $F_3(f)$, $F_{4+}(t)$ and $F_{5\pm}(t)$. The standard deviations in those cases are the same. The solid line and the dotted line are used for $+\sigma$ and $-\sigma$, respectively. Figure 19 (a) and (b) show accelerations estimated by AR model for the acceleration obtained by applying $F_1(f)$, $F_2(f)$, $F_3(f)$, $F_{4+}(t)$ and $F_{5+}(t)$, and by applying $F_1(f)$, $F_2(f)$, $F_3(f)$, $F_{4+}(t)$ and $F_{5-}(t)$, respectively. The difference of maximum amplitudes before and after applying $F_1(f)$, $F_2(f)$, $F_3(f)$, $F_{4+}(t)$, $F_{5+}(t)$ and the AR model is 2.31%. That before and after applying $F_1(f)$, $F_2(f)$, $F_3(f)$, $F_{4+}(t)$, $F_{5-}(t)$ and the AR model is 1.61%.

Therefore, the maximum and minimum differences of maximum amplitudes before and after applying ① to ⑥-1 processes are 2.44% and 1.48%, respectively. The differences are summarized in Table 4.

⑥-2 Process to estimate errors caused by disturbance using the LSAR model

In the LSAR model, any small segments in time series $y_1, \cdots, y_N$ are assumed to be represented by the AR model. The number of segments and the number of data in each segment are represented as k and N_i ($N_1 + \cdots + N_k = N$), respectively. The ith segment is represented as $[n_{i0}, n_{i1}]$. n_{i0} and n_{i1} are given as follows.

$$n_{i0} = \sum_{j=1}^{i-1} N_j + 1\,, \quad n_{i1} = \sum_{j=1}^{i} N_j \tag{14}$$

The LSAR model for jth segment is represented by Eq. (15).

$$y_n = \sum_{i=1}^{m_j} a_{ji} y_{n-i} + v_{nj} \tag{15}$$

Here, v_{nj} is a white noise with average zero and dispersion σ_j^2. $m_j = 10$ is chosen. A multiple of 32 is used for the period of each segment. In the same way as the AR model, substituting the acceleration data after applying $F_1(f)$, $F_2(f)$, $F_3(f)$, $F_{4\pm}(t)$ and $F_{5\pm}(t)$ for $y_1, \cdots, y_N$, errors caused by disturbance is estimated.

Figure 20 (a) and (b) show standard deviations $\pm\sigma$ when substituting the acceleration data after applying $F_1(f)$, $F_2(f)$, $F_3(f)$, $F_{4-}(t)$ and $F_{5\pm}(t)$. The solid line and the dotted line are used for $+\sigma$ and $-\sigma$, respectively. Symbols ⑥-2 is used for the process by the LSAR model. Figure 21 (a) and (b) show accelerations estimated by LSAR model for the acceleration obtained by applying $F_1(f)$, $F_2(f)$, $F_3(f)$, $F_{4-}(t)$ and $F_{5+}(t)$, and by applying $F_1(f)$, $F_2(f)$, $F_3(f)$, $F_{4-}(t)$ and $F_{5-}(t)$, respectively. The difference of maximum amplitude before and after applying $F_1(f)$, $F_2(f)$, $F_3(f)$, $F_{4-}(t)$, $F_{5+}(t)$ and the LSAR model is 3.37%. That before and after applying $F_1(f)$, $F_2(f)$, $F_3(f)$, $F_{4-}(t)$, $F_{5-}(t)$ and the LSAR model is 1.05%.

Figure 22 (a) and (b) show standard deviations $\pm\sigma$ when substituting the acceleration data after applying $F_1(f)$, $F_2(f)$, $F_3(f)$, $F_{4+}(t)$ and $F_{5\pm}(t)$. The solid line and the dotted line are used for $+\sigma$ and $-\sigma$, respectively. Figure 23 (a) and (b) show accelerations estimated by LSAR model for the acceleration obtained by applying $F_1(f)$, $F_2(f)$, $F_3(f)$, $F_{4+}(t)$ and $F_{5+}(t)$, and by applying $F_1(f)$, $F_2(f)$, $F_3(f)$, $F_{4+}(t)$ and $F_{5-}(t)$, respectively. The difference of maximum amplitudes before and after applying $F_1(f)$, $F_2(f)$, $F_3(f)$, $F_{4+}(t)$, $F_{5+}(t)$ and the LSAR model is 3.15%. That before and after applying $F_1(f)$, $F_2(f)$, $F_3(f)$, $F_{4+}(t)$, $F_{5-}(t)$ and the LSAR model is 1.27%.

Therefore, the maximum and minimum differences of maximum amplitudes before and after applying ① to ⑥-2 processes are 1.05% and 3.37%, respectively. The differences are summarized in Table 5.

Figures 24, 25, 26 and 27 show Fourier spectrums of the estimated acceleration by applying $F_1(f)$, $F_2(f)$, $F_3(f)$, $F_{4\pm}(t)$, $F_{5\pm}(t)$ (a), and the AR model and absolute values of difference of Fourier spectrums before and after applying the AR model (b). Figures 28, 29,

30 and 31 show Fourier spectrums of the estimated acceleration by applying $F_1(f)$, $F_2(f)$, $F_3(f)$, $F_{4\pm}(t)$, $F_{5\pm}(t)$ (a), and the LSAR model and absolute values of difference of Fourier spectrums before and after applying the LSAR model (b). The difference between results by applying the AR model and the LSAR model is small for all frequency range but a little bit larger from 0 to 10 Hz. The division to small segments in time series in the LSAR model causes more flat increase of the Fourier spectrum.

3.4.2 Evaluation of results from two time series analysis models (AR model and LSAR model)

We evaluate which model is more appropriate to estimate errors caused by disturbance. We assume the acceleration data observed before a seismic wave reaches the observation target (namely the HTTR building) as disturbance acceleration data. The acceleration data is compared with the estimated disturbance acceleration data obtained using the AR model and the LSAR model shown in section 3.4.1. We use the seismic motions of three earthquakes; the off Ibaraki Prefecture earthquake and the 3.11 aftershocks (No. 4, 6 and 7 in Tab. 1).

Figure 32 (a), (b) and (c) show time series of observed acceleration for earthquakes No. 4, 6 and 7, respectively. In each graph, acceleration data observed at all accelerometers installed in the HTTR building are simultaneously plotted. Time series before each seismic wave reaches the observation target are magnified in right graphs. From Fig. 32, it can be seen that the amplitude of disturbance acceleration becomes larger in case with the larger amplitude of acceleration of seismic wave.

Figures 33, 34 and 35 show time series of the standard deviation of (observed) disturbance acceleration (for $t \le 0$), white noise in the AR model (for $t \ge 0$), and white noise in the LSAR model (for $t \ge 0$) at the center of B3 floor (a) and (b), the south side of 1st floor (c) and (d) and the south side of 2nd floor (e) and (f) in the HTTR building for three seismic motions; No. 4, 6 and 7, respectively. The broken line, the long dashed short dashed line, the dotted line and the solid line are used for the standard deviation of (observed) disturbance acceleration, the white noise when using the AR model after applying $F_1(f)$, $F_2(f)$, $F_3(f)$, $F_{4+}(t)$ and $F_{5\pm}(t)$ ((a), (c) and (e)) or after applying $F_1(f)$, $F_2(f)$, $F_3(f)$, $F_{4-}(t)$ and $F_{5\pm}(t)$ ((b), (d) and (f)) and white noise when using LSAR model after applying $F_1(f)$, $F_2(f)$, $F_3(f)$, $F_{4+}(t)$ and $F_{5+}(t)$ ((a), (c) and (e)) or after applying $F_1(f)$, $F_2(f)$, $F_3(f)$, $F_{4-}(t)$ and $F_{5+}(t)$ ((b), (d) and (f)), and the white noise when using LSAR model after applying $F_1(f)$, $F_2(f)$, $F_3(f)$, $F_{4+}(t)$ and $F_{5-}(t)$ ((a), (c) and (e)) or after applying $F_1(f)$, $F_2(f)$, $F_3(f)$, $F_{4-}(t)$ and $F_{5-}(t)$ ((b), (d) and (f)).

To evaluate which model is more appropriate, the continuity between the standard deviation of disturbance acceleration and that of white noise in the AR model/LSAR model at $t = 0$ is confirmed. From those figures, it can be seen that the amplitude at $t = 0$ is more

continuous in most cases using the LSAR model. It means that the LSAR model is more appropriate to estimate errors caused by disturbance than the AR model.

However, the LSAR model is not always enough to estimate errors caused by disturbance, since the continuity at $t=0$ is not enough especially for the wave of No. 6. It seems that when the maximum acceleration becomes larger, the continuity becomes worse. However, the reason has not been clear enough. The results using the LSAR model depend on two parameters (the degree of autoregression and the period of each segment). For example, when the larger value for those parameters is used, the stationary becomes broader and the standard deviation of white noise is averaged. In this paper, the period of each segment is also automatically determined using a multiple of the fixed minimum period[9]. How to determine those parameters to get more desirable results is a future issue. There are various models for the time series analysis. The application of the other models is also a future issue.

3.5 Estimation of maximum error

We have estimated errors for the acceleration data in the NS direction observed at the center in the B3 floor, the south side in the 1st floor and the south side in the 2nd floor for four seismic motions; No. 4, 5, 6 and 7 in Table 1. The results are shown in Figs. 36, 37, 38 and Table 6.

Figures 36, 37 and 38 show the maximum acceleration vs. absolute values of error after applying $F_1(f)$, $F_2(f)$, $F_3(f)$, $F_{4\pm}(t)$ and $F_{5\pm}(t)$, $F_1(f)$, $F_2(f)$, $F_3(f)$, $F_{4\pm}(t)$, $F_{5\pm}(t)$ and the AR model, and $F_1(f)$, $F_2(f)$, $F_3(f)$, $F_{4\pm}(t)$, $F_{5\pm}(t)$ and the LSAR model, respectively. Table 6 shows lower and higher limits of error range in those figures. The lower and higher limits of error range are respectively minimum and maximum values among four cases ④(-) and ⑤(+), ④(-) and ⑤(-), ④(+) and ⑤(+), and ④(+) and ⑤(-). For example, when applying $F_1(f)$, $F_2(f)$, $F_3(f)$, $F_{4\pm}(t)$ and $F_{5\pm}(t)$, four cases correspond to $F_1(f)$, $F_2(f)$, $F_3(f)$, $F_{4-}(t)$ and $F_{5+}(t)$, $F_1(f)$, $F_2(f)$, $F_3(f)$, $F_{4-}(t)$ and $F_{5-}(t)$, $F_1(f)$, $F_2(f)$, $F_3(f)$, $F_{4+}(t)$ and $F_{5+}(t)$, and $F_1(f)$, $F_2(f)$, $F_3(f)$, $F_{4+}(t)$ and $F_{5-}(t)$.

From those figures and table, it can be seen that absolute values of error after applying the processes $F_1(f)$, $F_2(f)$, $F_3(f)$, $F_{4\pm}(t)$ and $F_{5\pm}(t)$ are less than 3% and do not so much dependent on the difference of the maximum acceleration. When applying the AR model (see Fig. 37) and the LSAR mode (see Fig. 38), several absolute values of error become larger but are less than 8% and 6%, respectively. It is considered that the estimation of errors caused by disturbance which is included in data measured by an observational system is as effective as that of the processes for the estimation of errors caused by measurement accuracy.

4. Conclusion

The approach to estimate errors included in observed acceleration data is proposed toward V&V of the seismic simulation for entire nuclear plant and is applied to the acceleration data observed in the HTTR building. To achieve those, we firstly define the relation between the process of V&V and the observed acceleration and consider that errors are caused by disturbance which is included in data measured by an observational system and measurement accuracy which is included in the observational system. Secondly, we examine error factors and consider that there are two factors for disturbance and that there are thirteen factors for measurement accuracy. Thirdly, we investigate methods to estimate those errors in existing researches and propose the approach to estimate errors by exploiting some of processes to estimate components regarded as errors in existing researches. We adopt each estimation technique appropriate to each item of the specification of an observational system for errors caused by measurement accuracy. In addition, we adopt time series analysis models for errors caused by disturbance. Accumulating techniques with considering the sequence in which errors are caused, total errors are estimated. To clarify the actual procedure, we apply the proposed approach to acceleration data observed in the HTTR building and estimate errors in the acceleration data. We use the acceleration data in the NS direction observed at the center of the B3 floor in the HTTR building for the seismic motion of off Ibaraki Prefecture earthquake occurred on October 19, 2005. As a result, it is found that after applying the LSAR model as the time series analysis, the maximum and minimum differences of maximum amplitudes are 3.37% and 1.05%, respectively. We also apply the approach to acceleration data in the NS direction observed at the center of the B3 floor, the south side of the 1st floor, and the south side of the 2nd floor in the HTTR building for seismic motions of off Ibaraki Prefecture earthquake occurred on October 19, 2005, off the Pacific coast of Tohoku occurred on March 11, 2011, 3.11 aftershock occurred on March 11, 2011, and 3.11 aftershock occurred on April 11, 2011. It is found that errors without and with the time series analysis (the LSAR model) are respectively under about 3% and 6% for maximum amplitudes of those seismic waves. It can be seen that the errors caused by disturbance is as effective as or less effective than ones caused by measurement accuracy which is included in an observational system.

The accelerometers were set in the HTTR building in 1997. However, specification items which is considered to influence error estimation are not so different for servo type accelerometers in recent years. Therefore, the errors we estimate in this paper would not be so reduced even if recent servo type accelerometers are used.

Acknowledgements

The author would like to thank members in Department of HTTR of Oarai Research and Development Institute of the Japan Atomic Energy Agency for supports and fruitful

discussions. This research is supported by the strategic programs for innovative research (the application 5 “Next-generation Seismic Simulation of Large Industrial Plants” in the field 4 “Industrial Innovation”) (Project ID: hp150207).

References

1) ASME Committee V&V 20, “Standard for Verification and Validation in Computational Fluid Dynamics and Heat Transfer”, ASME V&V 20-2009, American Society of Mechanical Engineers (2009).
2) Simulation Reliability Assessment Subcommittee in the Advanced and Fundamental Systems Technical Committee, the ATC and the Standards Committee, “Guideline for Credibility Assessment of Nuclear Simulations”, AESJ-SC-A008: 2015, Atomic Energy Society of Japan (2016).
3) Y. Suzuki, A. Nishida, F. Araya, N. Kushida, T. Akutsu, N. Teshima, K. Nakajima, M. Kondo, S. Hayashi, T. Aoyagi and N. Nakajima, “Development of Three-dimensional Virtual Plant Vibration Simulator on Grid Computing Environment ITBL-IS/AEGIS,” Journal of Power and Energy Systems, Vol. 3, No. 1, pp. 60-71 (2009).
4) Dept. of HTTR Project, “Design of High Temperature Engineering Test Reactor (HTTR)”, JAERI-1332, 247p. (1994).
5) S. Iai, E. Kurata and H. Tsuchida, “Digitization and Corrections of Strong-Motion Accelerograms”, Technical Note of the Port and Harbour Research Institute Ministry of Transport, Japan, No.286, Port and Harbour Research Institute, Japan (1978) [in Japanese].
6) A. Nozu, A. Wakai and Y. Nagasaka, “Annual Report on Strong-Motion Earthquake Records in Japanese Ports (2012)”, Technical Note of the Port and Airport Research Institute, No.1283, Port and Airport Research Institute, Japan (2014) [in Japanese].
7) S. Okada, “A Study into Renewal of Seismic Strong Motion Observation System -Part 1 Proposal of desired performance based upon critical examination of existing seismographs-”, Transactions of the Architectural Institute of Japan, No. 339, pp. 45-56 (1984) [in Japanese].
8) Y. Suzuki, Y. Kawakami and N. Nakajima, “Investigation of error estimation method of observational data and comparison method between numerical and observational results toward V&V of seismic simulation”, Mechanical Engineering Reviews, Vol. 4, No. 1, pp.1-18 (2017).
9) G. Kitagawa, “Jikeiretsu Kaiseki Nyuumon”, Iwanami-Shoten, ISBN 978-4000054553 (2005) [in Japanese].
10) G. Kitagawa Ed., “Jikeiretsu Kaiseki no Jissai (1)”, Asakura-Shoten, ISBN 978-4254125832 (1994) [in Japanese].
11) G. Kitagawa Ed., “Jikeiretsu Kaiseki no Jissai (2)”, Asakura-Shoten, ISBN 978-

4254125849 (1995) [in Japanese].

12) Y. Inagaki, “Experimental study on flow-induced vibration and heat transfer characteristics of heat exchanger with helically coiled tube bundles”, JAERI-Research 97-069, 31p. (1997) [in Japanese].

13) M. Kondo, K. Iigaki, T. Motegi, and K. Emori, “Maintenance of seismic observation systems in HTTR”, JAEA-Testing 2009-002, 50p. (2009) [in Japanese].

14) N. Nakajima, Y. Suzuki, H. N. Miyamura, A. Nishida, Y. Kawakami, Z. Guo and E. Tomiyama, “An illustration by the next generation numerical simulator for quake-proofing on the K”, Journal of the Japan Society for Computational Engineering and Science, Vol. 20, No. 4, pp. 3338-3340 (2015) [in Japanese].

15) W. R. Bennett, “Spectra of Quantized Signals”, Bell System Technical Journal, Vol. 27, No. 3, pp. 446-471 (1948).

16) H. Goto, H. Kameda, M. Sugito and N. Imanishi, “Correction of SMAC-B2 Accelerograph Records by Digital Filter”, Proceedings of the Japan Society of Civil Engineers, No. 277, pp. 57-69 (1978) [in Japanese].

Table 1 Target seismic motions.

No.	Region	Date (Time)	Max. Acc. [cm/s^2]	Magnitude
1	-	1988.04.09 (17:45)	92.3	M5.4
2	Northern Ibaraki Prefecture	1989.03.26 (08:31)	110.7	M5.0
3	-	1989.04.25 (21:27)	77.8	M5.2
4	Off Ibaraki Prefecture	2005.10.19 (20:44)	78.4	M6.3
5	Off the Pacific coast of Tohoku	2011.03.11 (14:46)	558.3	M9.0
6	3.11 aftershock	2011.03.11 (15:15)	382.9	M7.6
7	3.11 aftershock	2011.04.11 (17.16)	179.6	M7.0

Table 2 Specification items of the observational system in HTTR.

Item	Seismometer	Transmission Equipment	Recording Equipment
Full scale (FS)	±11V	±2000cm/s^2±11V	±10V
Frequency	0～50Hz	0～100Hz	-
Linearity	0.0015% (FS)	0.03% (FS)	-
Quantized frequency	100, 200Hz	-	50, 100, 200Hz
Sensitivity	-	5mV/cm/s^2	-
Resolution	～0.3mV	～0.001cm/s^2	-
A/D conversion	16bit	-	16bit
Temperature coefficient for sensitivity	-	0.01%/℃	-
Temperature coefficient for zero shift	-	0.05%/℃	-
Transverse sensitivity	-	0.008G/G	-
Filter	LPF 33Hz-8db/Oct	-	LPF 30.5Hz-24db/Oct Butterworth

Table 3 Differences of maximum amplitudes before and after applying $F_1(f)$, $F_2(f)$, $F_3(f)$, $F_{4\pm}(t)$ and $F_{5\pm}(t)$, and the maximum and minimum differences of maximum amplitudes.

case	Difference of max. amplitudes (%)
Difference before and after applying $F_1(f)$, $F_2(f)$, $F_3(f)$, $F_{4-}(t)$ and $F_{5+}(t)$	1.36
Difference before and after applying $F_1(f)$, $F_2(f)$, $F_3(f)$, $F_{4-}(t)$ and $F_{5-}(t)$	2.95
Difference before and after applying $F_1(f)$, $F_2(f)$, $F_3(f)$, $F_{4+}(t)$ and $F_{5+}(t)$	1.25
Difference before and after applying $F_1(f)$, $F_2(f)$, $F_3(f)$, $F_{4+}(t)$ and $F_{5-}(t)$	3.06
minimum difference	1.25
maximum difference	3.06

Table 4 Differences of maximum amplitudes before and after applying $F_1(f)$, $F_2(f)$, $F_3(f)$, $F_{4\pm}(t)$, $F_{5\pm}(t)$ and the AR model, and the maximum and minimum differences of maximum amplitudes.

case	Difference of max. amplitudes (%)
Difference before and after applying $F_1(f)$, $F_2(f)$, $F_3(f)$, $F_{4-}(t)$, $F_{5+}(t)$ and the AR model	2.44
Difference before and after applying $F_1(f)$, $F_2(f)$, $F_3(f)$, $F_{4-}(t)$, $F_{5-}(t)$ and the AR model	1.48
Difference before and after applying $F_1(f)$, $F_2(f)$, $F_3(f)$, $F_{4+}(t)$, $F_{5+}(t)$ and the AR model	2.31
Difference before and after applying $F_1(f)$, $F_2(f)$, $F_3(f)$, $F_{4+}(t)$, $F_{5-}(t)$ and the AR model	1.61
minimum difference	1.48
maximum difference	2.44

Table 5 Differences of maximum amplitudes before and after applying $F_1(f)$, $F_2(f)$, $F_3(f)$, $F_{4\pm}(t)$, $F_{5\pm}(t)$ and the LSAR model, and the maximum and minimum differences of maximum amplitudes.

case	Difference of max. amplitudes (%)
Difference before and after applying $F_1(f)$, $F_2(f)$, $F_3(f)$, $F_{4-}(t)$, $F_{5+}(t)$ and the LSAR model	3.37
Difference before and after applying $F_1(f)$, $F_2(f)$, $F_3(f)$, $F_{4-}(t)$, $F_{5-}(t)$ and the LSAR model	1.05
Difference before and after applying $F_1(f)$, $F_2(f)$, $F_3(f)$, $F_{4+}(t)$, $F_{5+}(t)$ and the LSAR model	3.15
Difference before and after applying $F_1(f)$, $F_2(f)$, $F_3(f)$, $F_{4+}(t)$, $F_{5-}(t)$ and the LSAR model	1.27
minimum difference	1.05
maximum difference	3.37

Table 6 Error ranges (%) for four seismic motions No. 4, 5, 6 and 7.

No.	Location	①②③④⑤	①②③④⑤⑥-1	①②③④⑤⑥-2
4	Center in the B3 floor	1.25～3.06	1.48～2.44	1.05～3.37
4	South side in the 1st floor	1.13～1.79	0.47～2.84	0.00～3.18
4	South side in the 2nd floor	0.52～1.77	0.19～1.51	0.03～2.35
5	Center in the B3 floor	0.35～1.56	0.15～1.78	0.31～1.53
5	South side in the 1st floor	0.05～1.63	2.24～3.59	0.89～2.48
5	South side in the 2nd floor	0.83～1.99	1.85～2.72	4.25～5.55
6	Center in the B3 floor	0.31～2.81	0.08～1.34	3.85～5.71
6	South side in the 1st floor	1.38～2.85	3.53～4.58	0.15～1.45
6	South side in the 2nd floor	1.24～2.46	6.51～7.32	3.97～5.04
7	Center in the B3 floor	0.59～1.48	0.00～0.77	2.28～3.08
7	South side in the 1st floor	1.88～2.40	1.25～1.60	3.09～3.72
7	South side in the 2nd floor	2.16～2.65	6.97～7.36	4.63～5.16

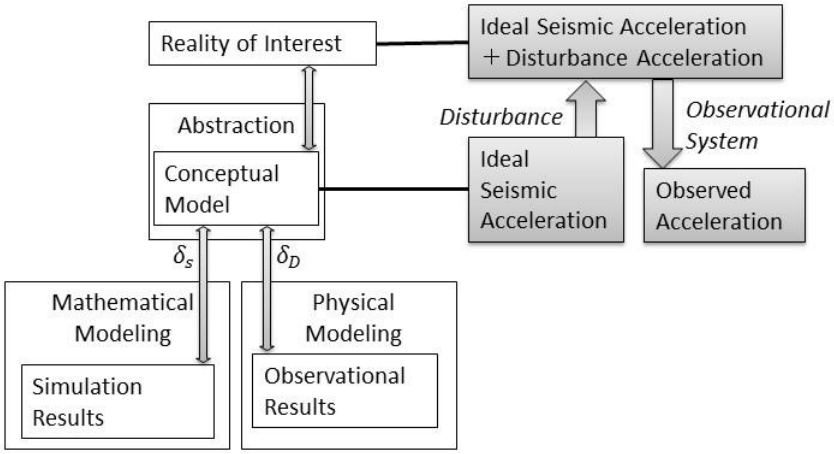

Fig.1 Placement of various acceleration data in process of V&V.

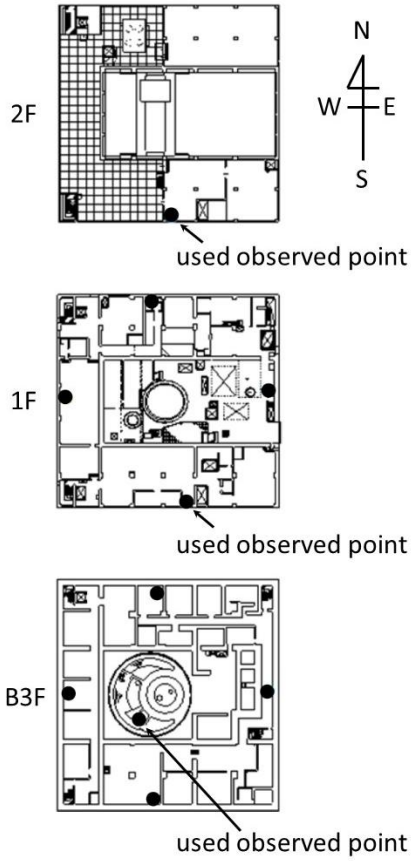

Fig.2 Used observed points, which are the center of B3 floor, the south side of 1st floor, and the south side of 2nd floor in HTTR building, are shown.
(Those diagrams are partly modified from the viewpoint of the physical protection of nuclear material.)

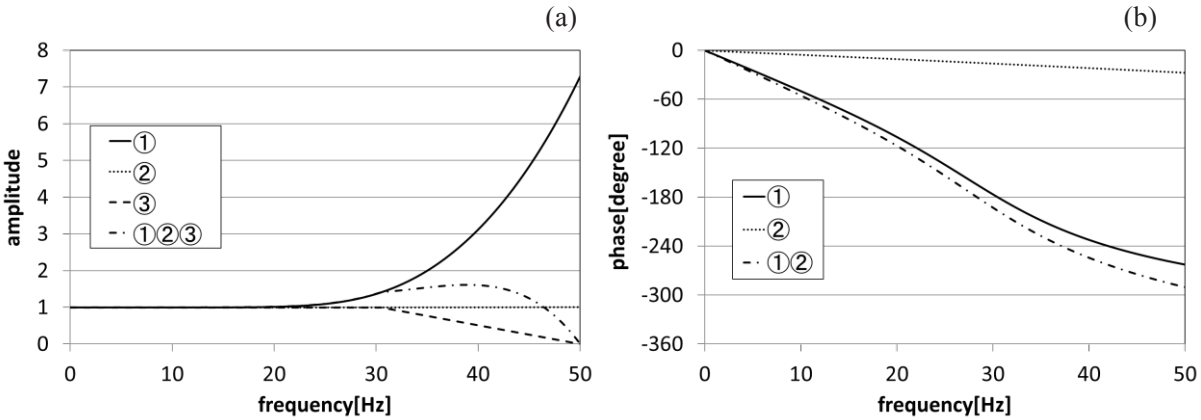

Fig. 3 Amplitudes $1/A_1$ (①), $1/A_2$ (②), A_3 (③) and $1/A = A_3/(A_1 \cdot A_2)$ (①②③) (a), and phases ϕ_1 (①), ϕ_2 (②) and $\phi = \emptyset_1 + \emptyset_2$ (①②) (b).

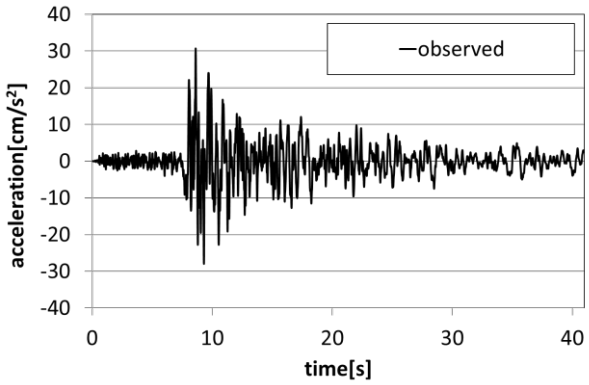

Fig. 4 Time series of the observed acceleration (indicated by "observed").

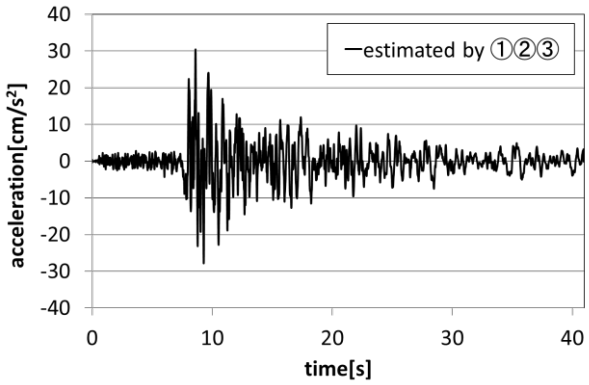

Fig. 5 Time series of the estimated acceleration by applying $F_1(f)$, $F_2(f)$ and $F_3(f)$ (indicated by "estimated by ①②③").

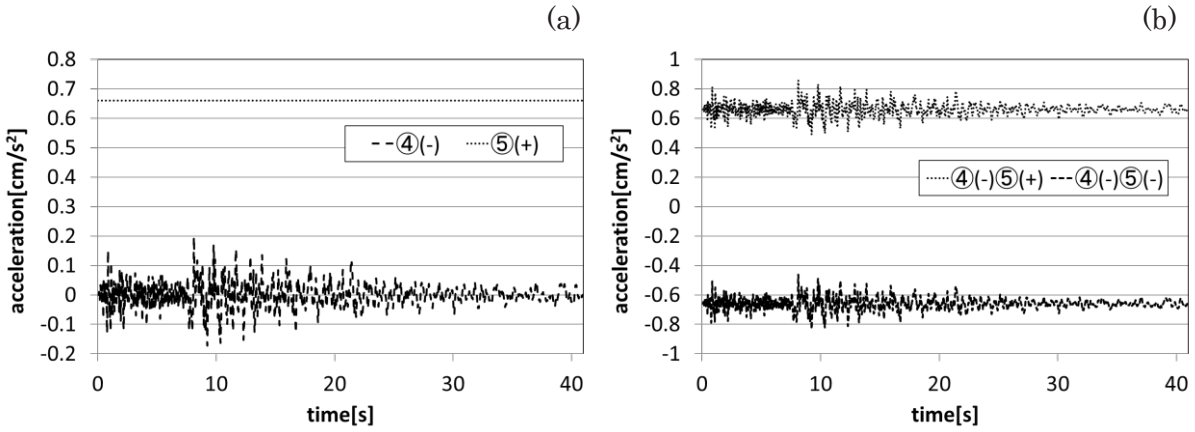

Fig. 6 Time series of errors by $F_{4-}(t)$ (④(-)) and $F_{5+}(t)$ (⑤(+)) (a), the combination of $F_{4-}(t)$ and $F_{5+}(t)$ (④(-)⑤(+)), and the combination of $F_{4-}(t)$ and $F_{5-}(t)$ (④(-)⑤(-)) (b).

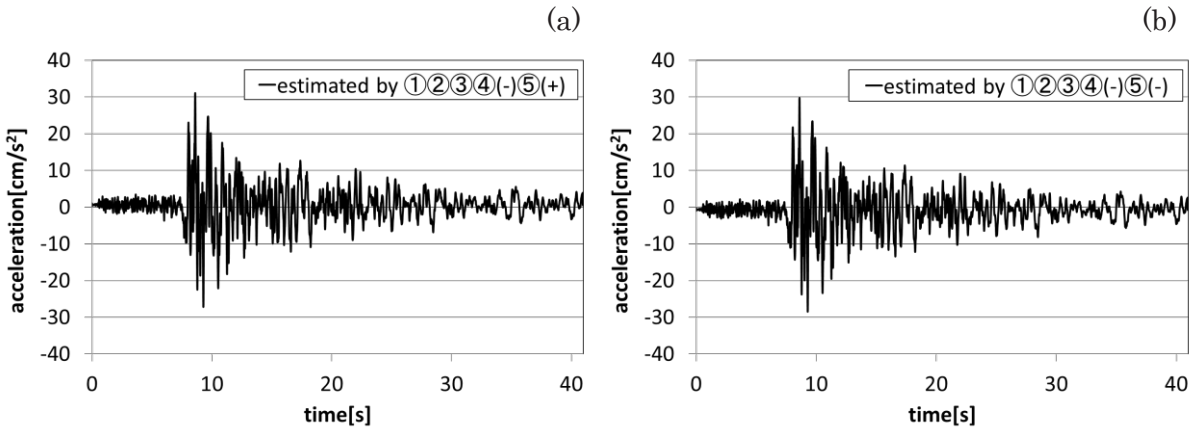

Fig. 7 Time series of the estimated accelerations by applying $F_1(f)$, $F_2(f)$, $F_3(f)$, $F_{4-}(t)$ and $F_{5+}(t)$ (estimated by ①②③④(-)⑤(+)) (a), and $F_1(f)$, $F_2(f)$, $F_3(f)$, $F_{4-}(t)$ and $F_{5-}(t)$ (estimated by ①②③④(-)⑤(-)) (b).

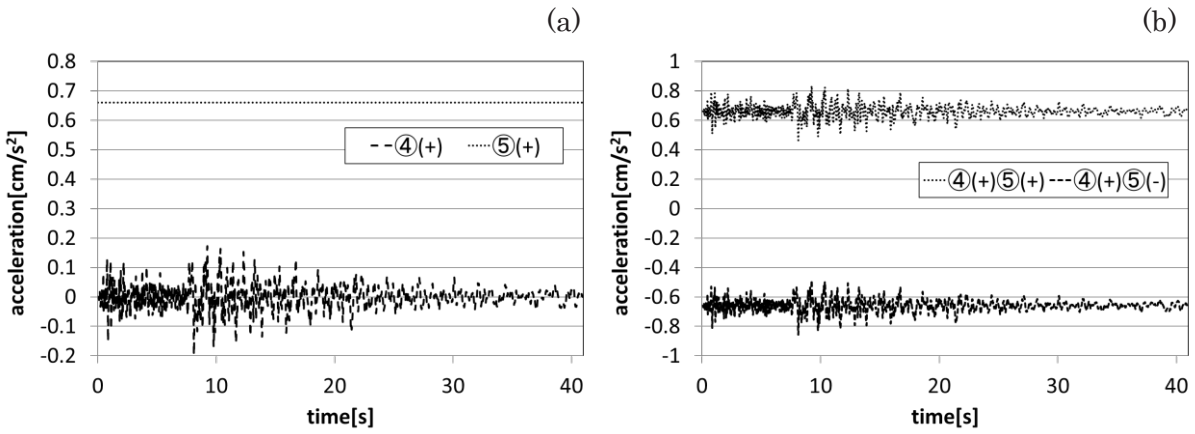

Fig. 8 Time series of errors by $F_{4+}(t)$ (④(+)) and $F_{5+}(t)$ (⑤(+)) (a), the combination of $F_{4+}(t)$ and $F_{5+}(t)$ (④(+)⑤(+)), and the combination of $F_{4+}(t)$ and $F_{5-}(t)$ (④(+)⑤(-)) (b).

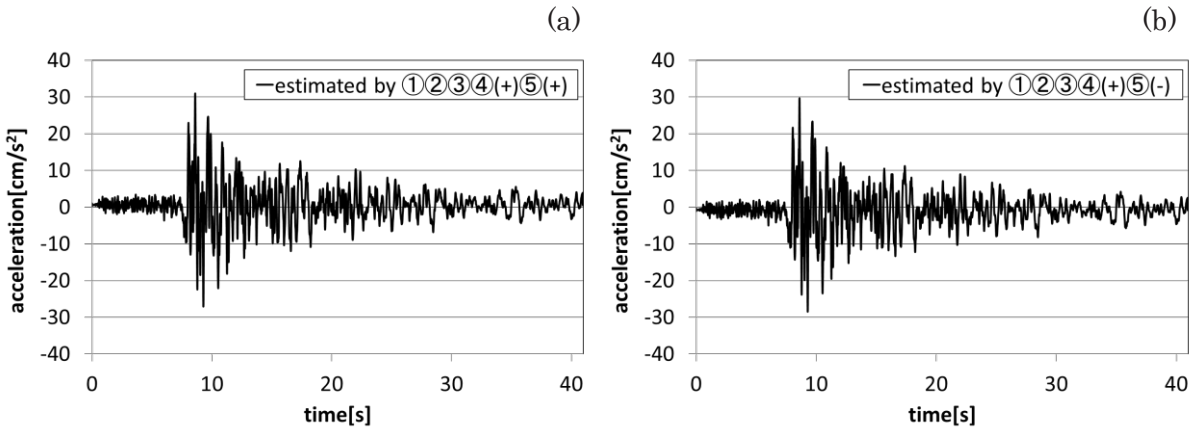

Fig. 9 Time series of the estimated accelerations by applying $F_1(f)$, $F_2(f)$, $F_3(f)$, $F_{4+}(t)$ and $F_{5+}(t)$ (estimated by ①②③④(+)⑤(+)) (a), and $F_1(f)$, $F_2(f)$, $F_3(f)$, $F_{4+}(t)$ and $F_{5-}(t)$ (estimated by ①②③④(+)⑤(-)) (b).

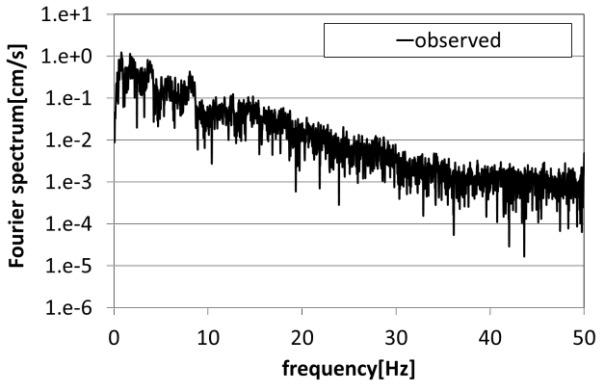

Fig. 10 Fourier spectrum of the observed acceleration.

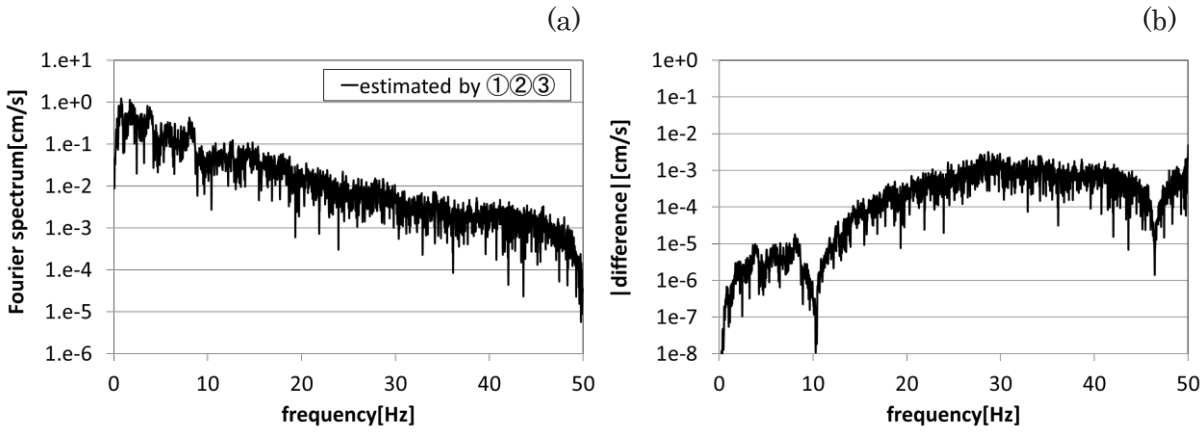

Fig. 11 Fourier spectrum of the estimated acceleration by applying $F_1(f)$, $F_2(f)$ and $F_3(f)$ (estimated by ①②③) (a), and the absolute value of difference of Fourier spectrums before and after applying $F_1(f)$, $F_2(f)$ and $F_3(f)$ (b).

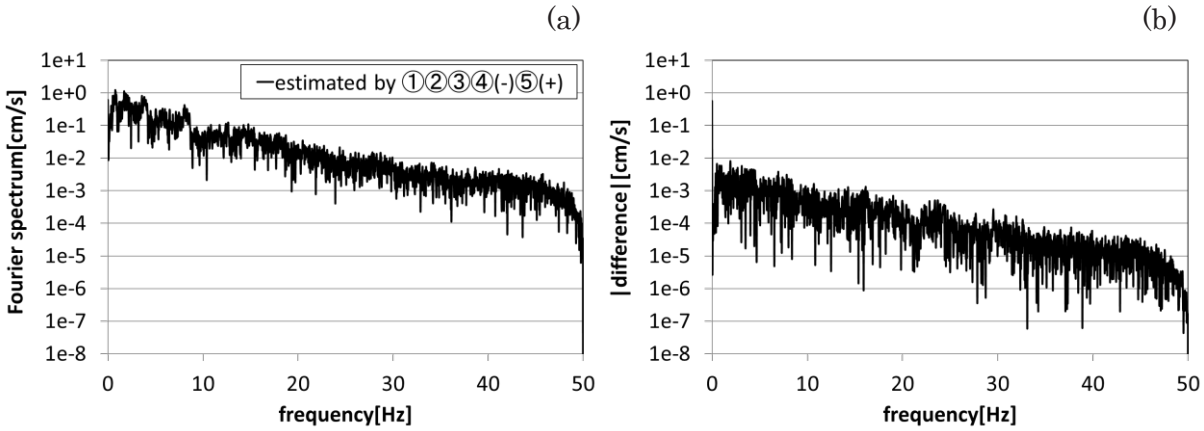

Fig. 12 Fourier spectrum of the estimated acceleration by applying $F_1(f)$, $F_2(f)$, $F_3(f)$, $F_{4-}(t)$ and $F_{5+}(t)$ (estimated by ①②③④(-)⑤(+)) (a), and the absolute value of difference of Fourier spectrums before and after applying $F_{4-}(t)$ and $F_{5+}(t)$ (b).

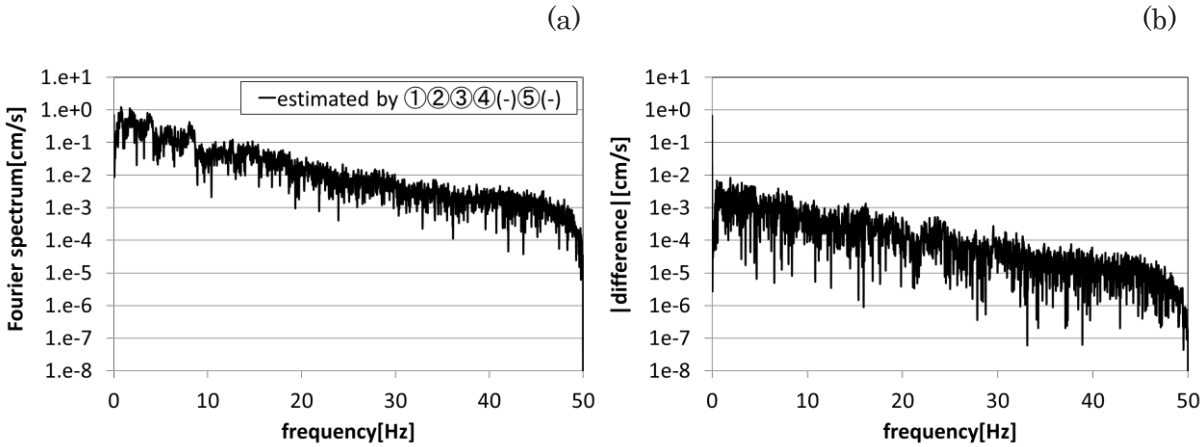

Fig. 13 Fourier spectrum of the estimated acceleration by applying $F_1(f)$, $F_2(f)$, $F_3(f)$, $F_{4-}(t)$ and $F_{5-}(t)$ (estimated by ①②③④(-)⑤(-)) (a), and the absolute value of difference of Fourier spectrums before and after applying $F_{4-}(t)$ and $F_{5-}(t)$ (b).

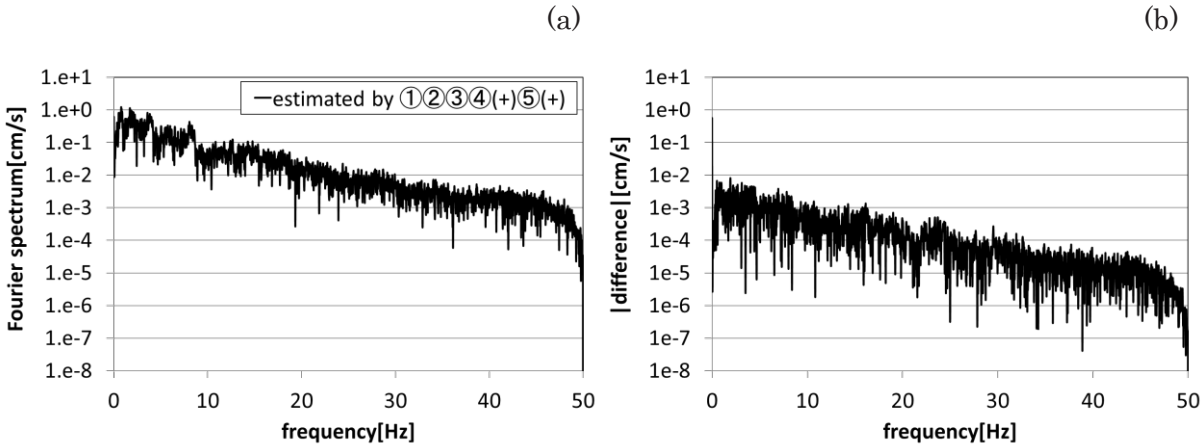

Fig. 14 Fourier spectrum of the estimated acceleration by applying $F_1(f)$, $F_2(f)$, $F_3(f)$, $F_{4+}(t)$ and $F_{5+}(t)$ (estimated by ①②③④(+)⑤(+)) (a), and the absolute value of difference of Fourier spectrums before and after applying $F_{4+}(t)$ and $F_{5+}(t)$ (b).

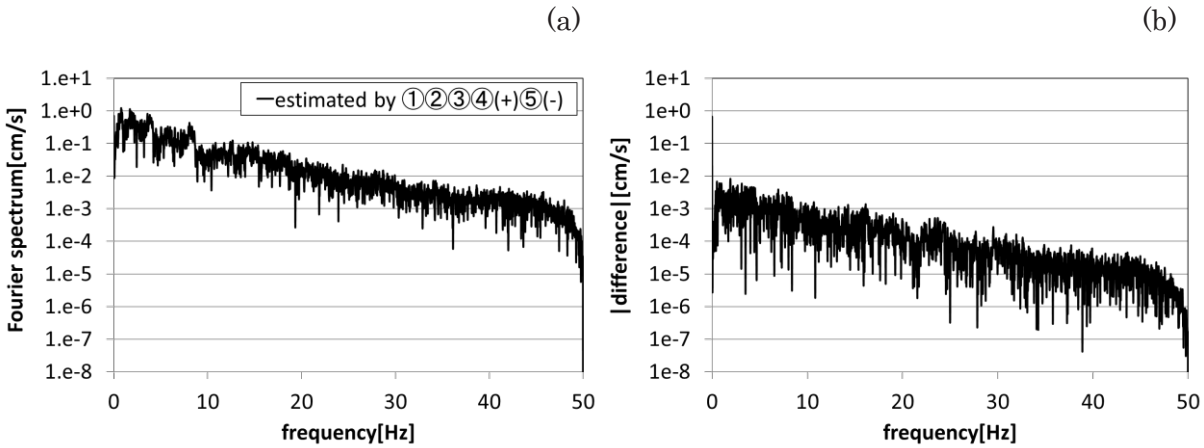

Fig. 15 Fourier spectrum of the estimated acceleration by applying $F_1(f)$, $F_2(f)$, $F_3(f)$, $F_{4+}(t)$ and $F_{5-}(t)$ (estimated by ①②③④(+)⑤(-)) (a), and the absolute value of difference of Fourier spectrums before and after applying $F_{4+}(t)$ and $F_{5-}(t)$ (b).

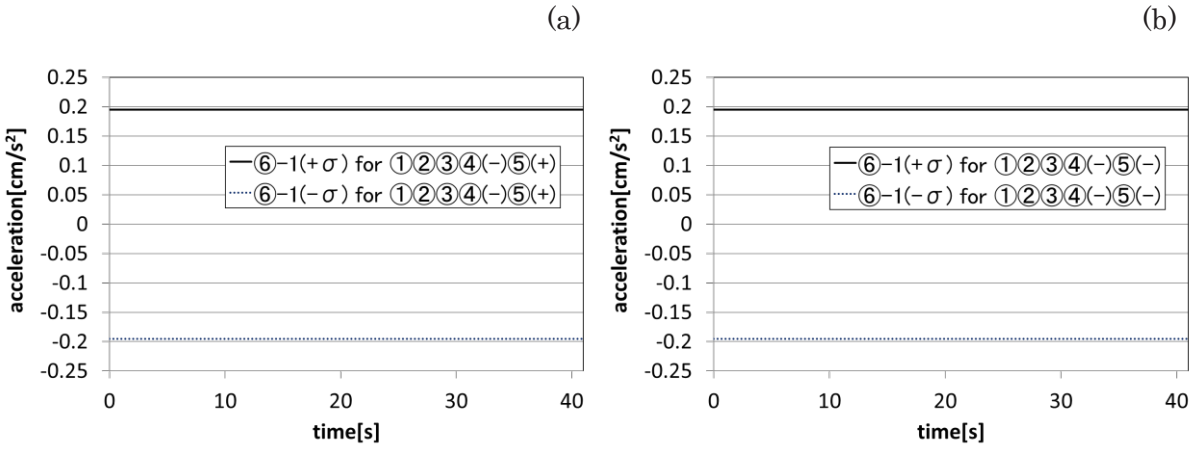

Fig. 16 Time series of the standard deviation estimated by applying the AR model for accelerations obtained by using $F_1(f)$, $F_2(f)$, $F_3(f)$, $F_{4-}(t)$ and $F_{5+}(t)$ (⑥-1(±σ) for ①②③④(-)⑤(+)) (a), and using $F_1(f)$, $F_2(f)$, $F_3(f)$, $F_{4-}(t)$ and $F_{5-}(t)$ (⑥-1(±σ) for ①②③④(-)⑤(-)) (b).

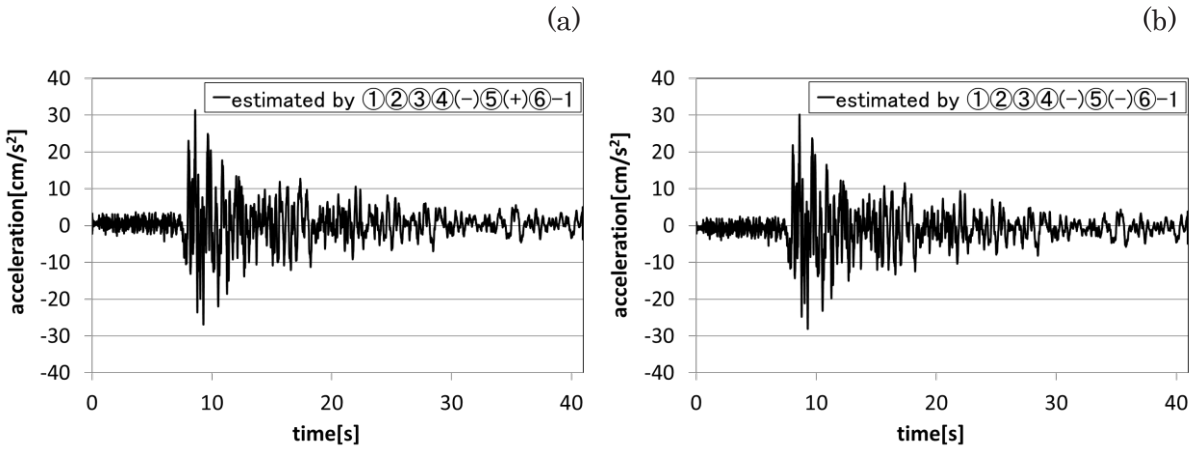

Fig. 17 Time series of accelerations estimated by applying the AR model for accelerations obtained by using $F_1(f)$, $F_2(f)$, $F_3(f)$, $F_{4-}(t)$ and $F_{5+}(t)$ (estimated by ①②③④(-)⑤(+)⑥-1) (a), and using $F_1(f)$, $F_2(f)$, $F_3(f)$, $F_{4-}(t)$ and $F_{5-}(t)$ (estimated by ①②③④(-)⑤(-)⑥-1) (b).

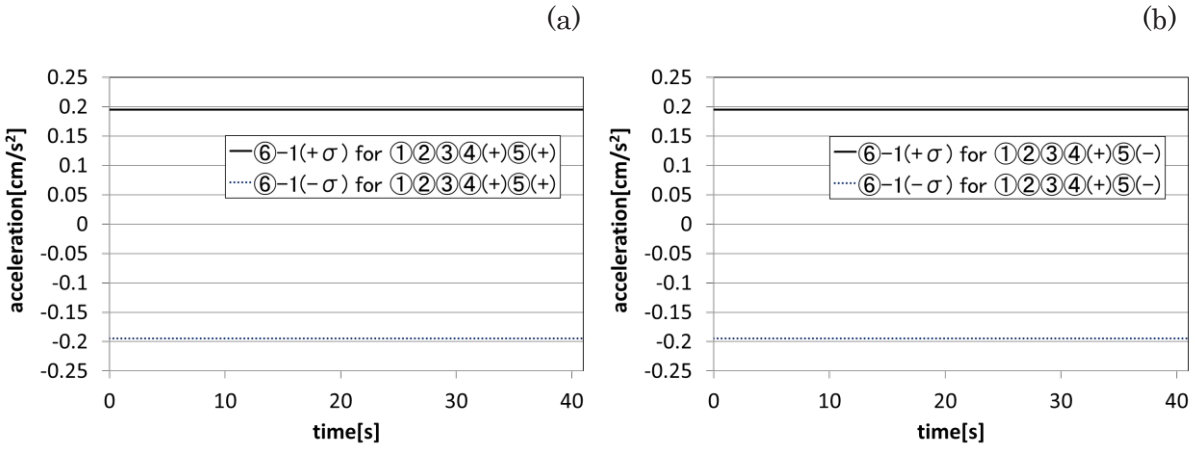

Fig. 18 Time series of the standard deviation estimated by applying the AR model for accelerations obtained by using $F_1(f)$, $F_2(f)$, $F_3(f)$, $F_{4+}(t)$ and $F_{5+}(t)$ (⑥-1(±σ) for ①②③④(+)⑤(+)) (a), and using $F_1(f)$, $F_2(f)$, $F_3(f)$, $F_{4+}(t)$ and $F_{5-}(t)$ (⑥-1(±σ) for ①②③④(+)⑤(-)) (b).

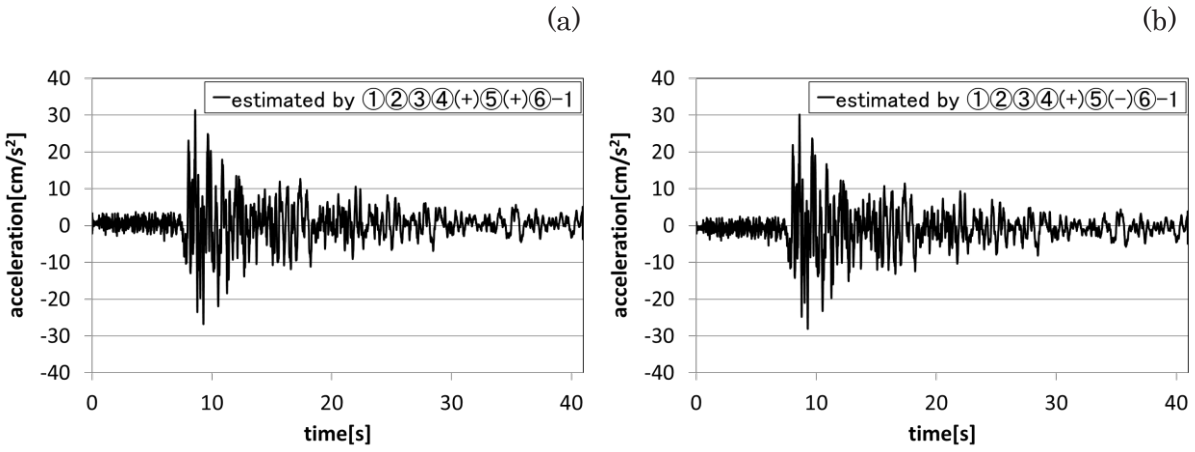

Fig. 19 Time series of accelerations estimated by applying the AR model for accelerations obtained by using $F_1(f)$, $F_2(f)$, $F_3(f)$, $F_{4+}(t)$ and $F_{5+}(t)$ (estimated by ①②③④(+)⑤(+)⑥-1) (a), and using $F_1(f)$, $F_2(f)$, $F_3(f)$, $F_{4+}(t)$ and $F_{5-}(t)$ (estimated by ①②③④(+)⑤(-)⑥-1) (b).

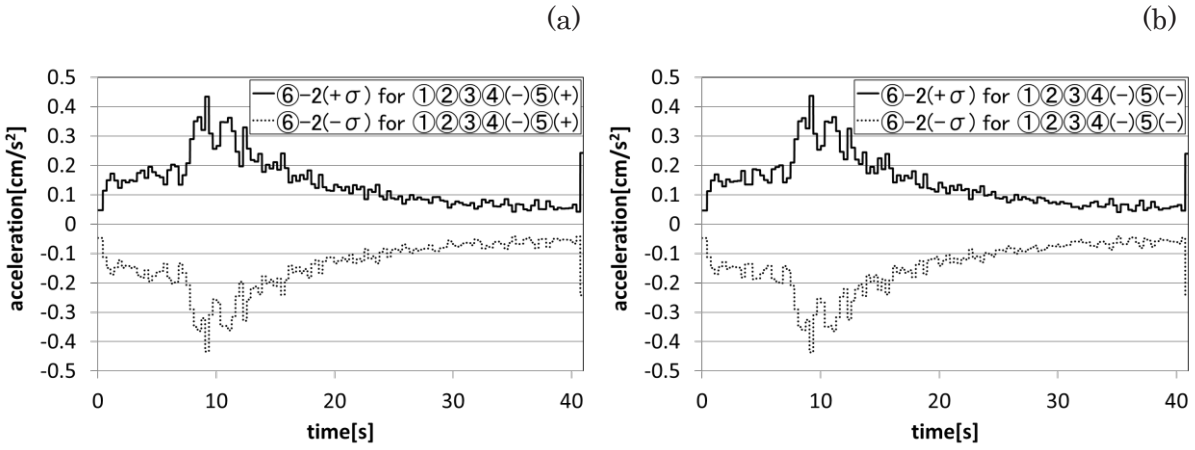

Fig. 20 Time series of the standard deviation estimated by applying the LSAR model for accelerations obtained by using $F_1(f)$, $F_2(f)$, $F_3(f)$, $F_{4-}(t)$ and $F_{5+}(t)$ (⑥-2(±σ) for ①②③④(-)⑤(+)) (a), and using $F_1(f)$, $F_2(f)$, $F_3(f)$, $F_{4-}(t)$ and $F_{5-}(t)$ (⑥-2(±σ) for ①②③④(-)⑤(-)) (b).

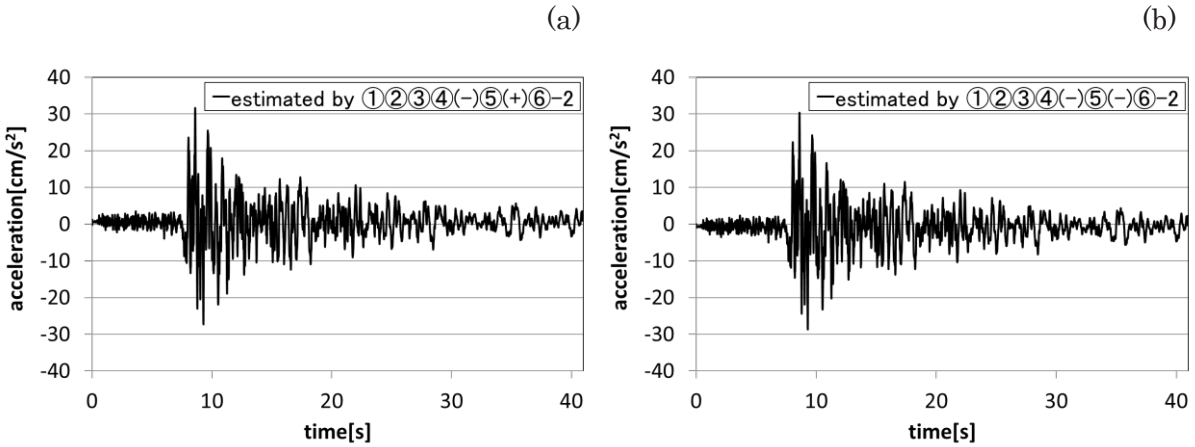

Fig. 21 Time series of accelerations estimated by applying the LSAR model for accelerations obtained by using $F_1(f)$, $F_2(f)$, $F_3(f)$, $F_{4-}(t)$ and $F_{5+}(t)$ (estimated by ①②③④(-)⑤(+)⑥-2) (a), and using $F_1(f)$, $F_2(f)$, $F_3(f)$, $F_{4-}(t)$ and $F_{5-}(t)$ (estimated by ①②③④(-)⑤(-)⑥-2) (b).

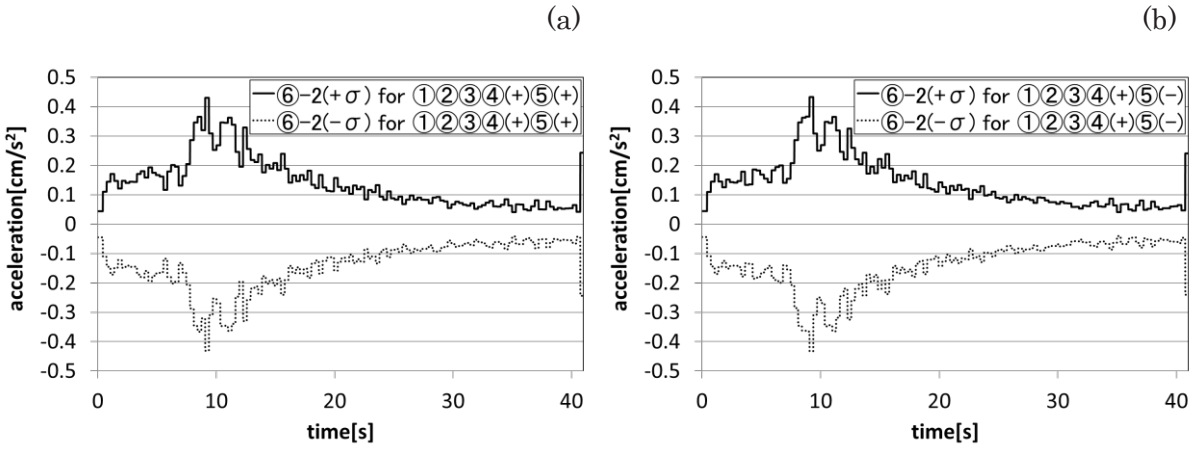

Fig. 22 Time series of the standard deviation estimated by applying the LSAR model for accelerations obtained by using $F_1(f)$, $F_2(f)$, $F_3(f)$, $F_{4+}(t)$ and $F_{5+}(t)$ (⑥-2(±σ) for ①②③④(+)⑤(+)) (a), and using $F_1(f)$, $F_2(f)$, $F_3(f)$, $F_{4+}(t)$ and $F_{5-}(t)$ (⑥-2(±σ) for ①②③④(+)⑤(-)) (b).

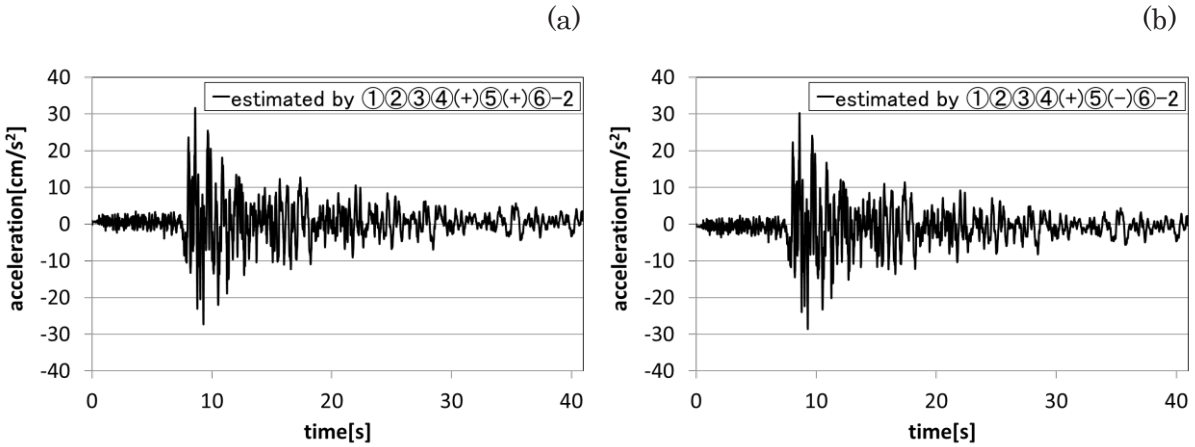

Fig. 23 Time series of accelerations estimated by applying the LSAR model for accelerations obtained by using $F_1(f)$, $F_2(f)$, $F_3(f)$, $F_{4+}(t)$ and $F_{5+}(t)$ (estimated by ①②③④(+)⑤(+)⑥-2) (a), and using $F_1(f)$, $F_2(f)$, $F_3(f)$, $F_{4+}(t)$ and $F_{5-}(t)$ (estimated by ①②③④(+)⑤(-)⑥-2) (b).

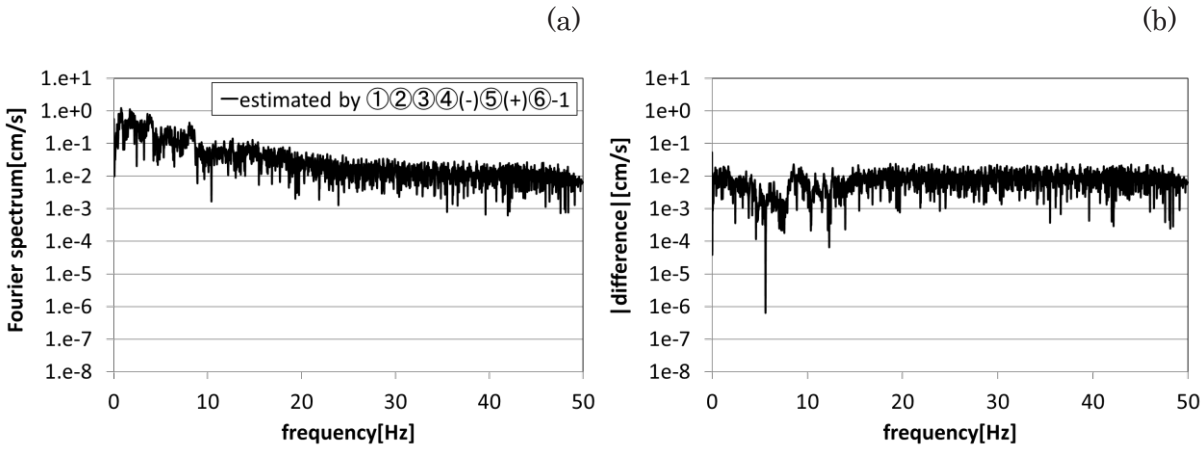

Fig. 24 Fourier spectrum of the estimated acceleration by applying $F_1(f)$, $F_2(f)$, $F_3(f)$, $F_{4-}(t)$, $F_{5+}(t)$ and the AR model (estimated by ①②③④(-)⑤(+)⑥-1) (a), and the absolute value of difference of Fourier spectrums before and after applying the AR model (b).

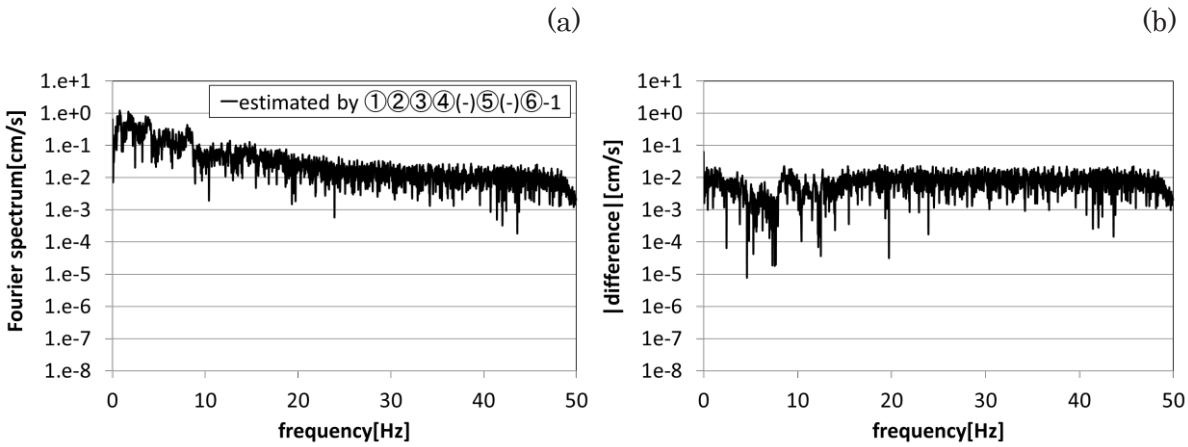

Fig. 25 Fourier spectrum of the estimated acceleration by applying $F_1(f)$, $F_2(f)$, $F_3(f)$, $F_{4-}(t)$, $F_{5-}(t)$ and the AR model (estimated by ①②③④(-)⑤(-)⑥-1) (a), and the absolute value of difference of Fourier spectrums before and after applying the AR model (b).

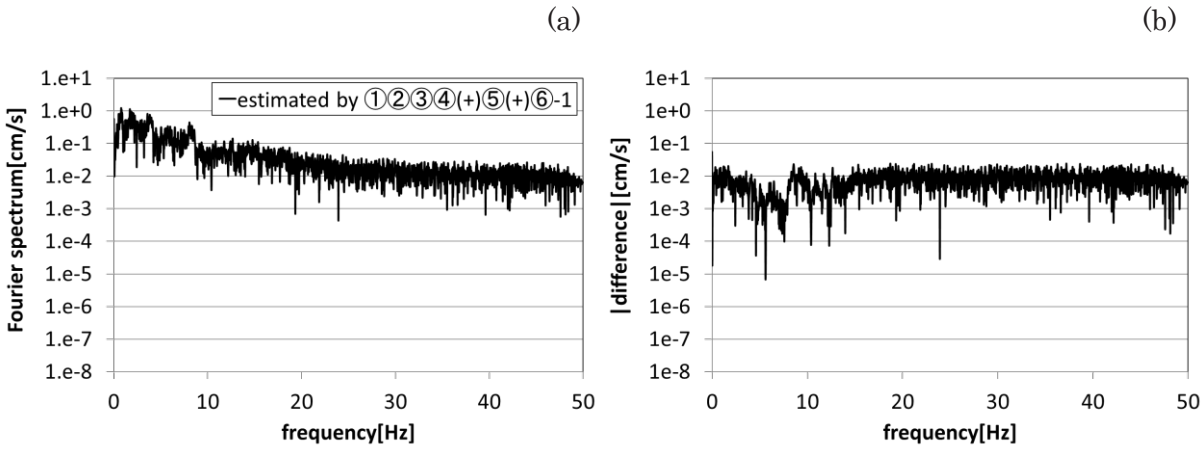

Fig. 26 Fourier spectrum of the estimated acceleration by applying $F_1(f)$, $F_2(f)$, $F_3(f)$, $F_{4+}(t)$, $F_{5+}(t)$ and the AR model (estimated by ①②③④(+)⑤(+)⑥-1) (a), and the absolute value of difference of Fourier spectrums before and after applying the AR model (b).

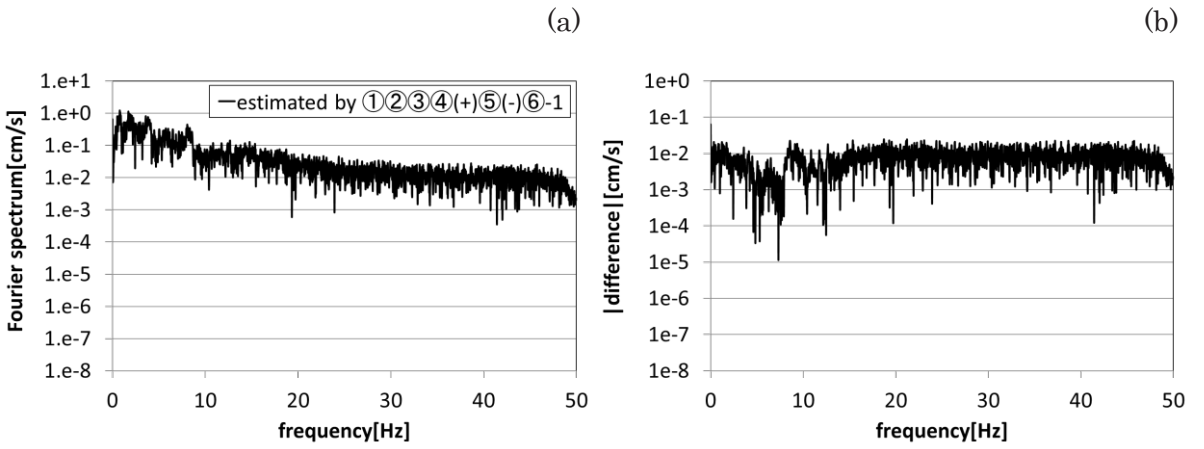

Fig. 27 Fourier spectrum of the estimated acceleration by applying $F_1(f)$, $F_2(f)$, $F_3(f)$, $F_{4+}(t)$, $F_{5-}(t)$ and the AR model (estimated by ①②③④(+)⑤(-)⑥-1) (a), and the absolute value of difference of Fourier spectrums before and after applying the AR model (b).

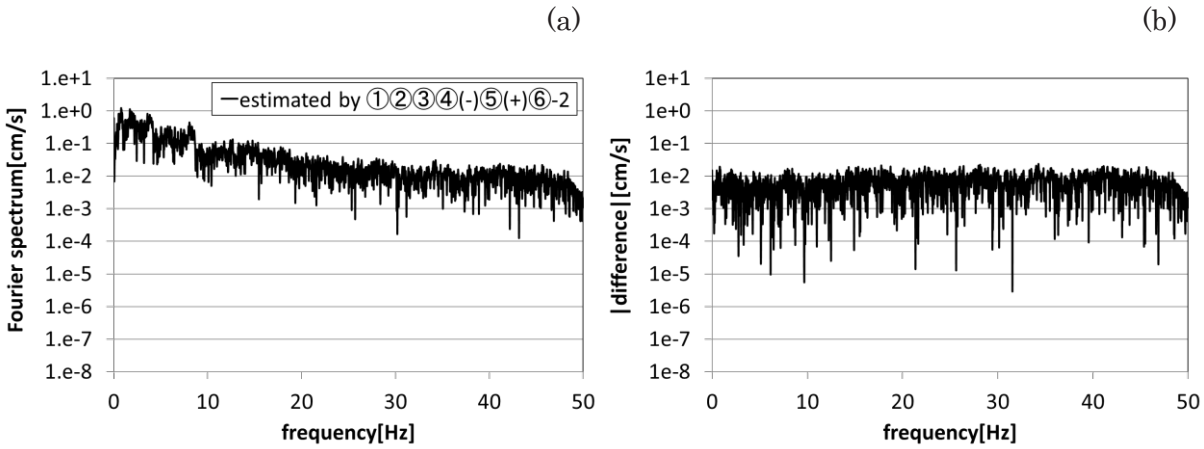

Fig. 28 Fourier spectrum of the estimated acceleration by applying $F_1(f)$, $F_2(f)$, $F_3(f)$, $F_{4-}(t)$, $F_{5+}(t)$ and the LSAR model (estimated by ①②③④(-)⑤(+)⑥-2) (a), and the absolute value of difference of Fourier spectrums before and after applying the LSAR model (b).

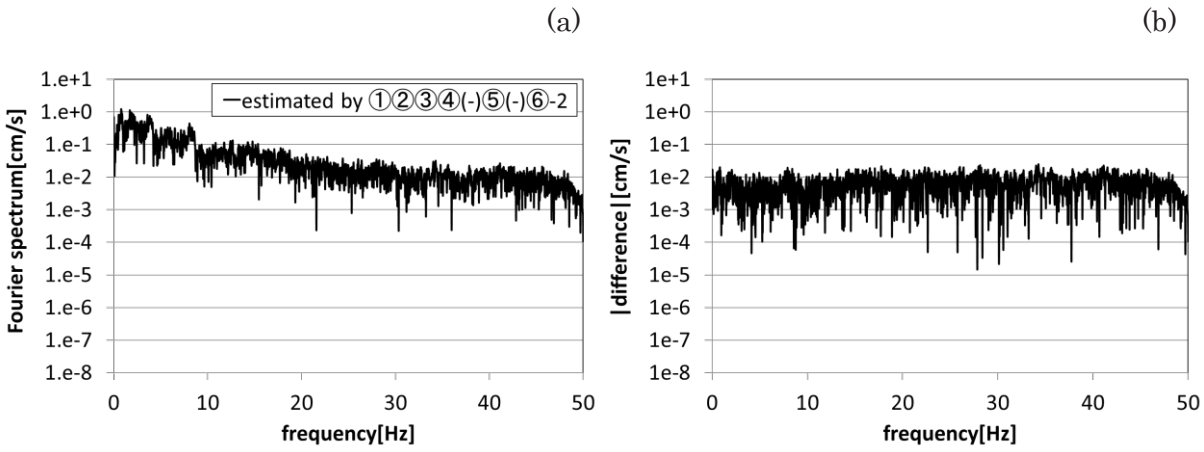

Fig. 29 Fourier spectrum of the estimated acceleration by applying $F_1(f)$, $F_2(f)$, $F_3(f)$, $F_{4-}(t)$, $F_{5-}(t)$ and the LSAR model (estimated by ①②③④(-)⑤(-)⑥-2) (a), and the absolute value of difference of Fourier spectrums before and after applying the LSAR model (b).

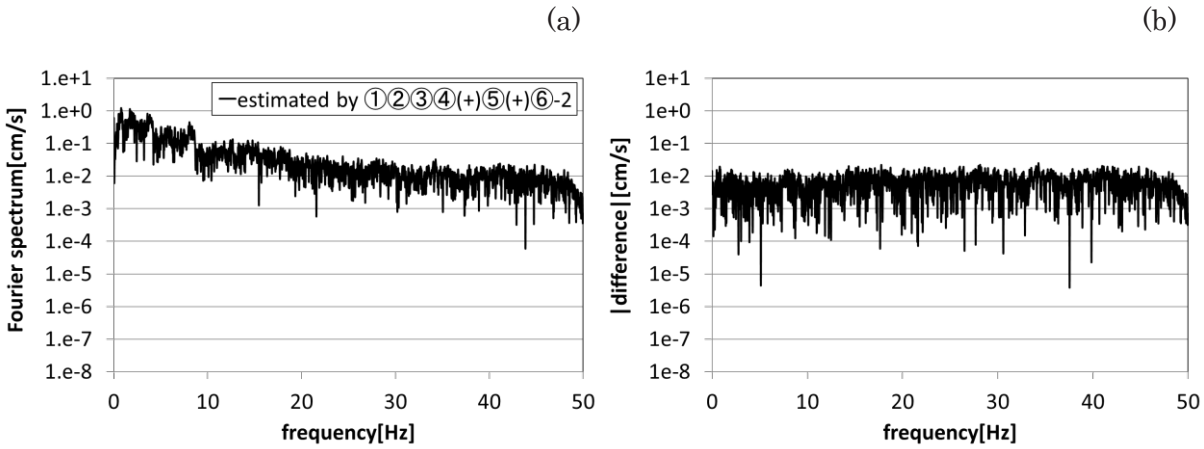

Fig. 30 Fourier spectrum of the estimated acceleration by applying $F_1(f)$, $F_2(f)$, $F_3(f)$, $F_{4+}(t)$, $F_{5+}(t)$ and the LSAR model (estimated by ①②③④(+)⑤(+)⑥-2) (a), and the absolute value of difference of Fourier spectrums before and after applying the LSAR model (b).

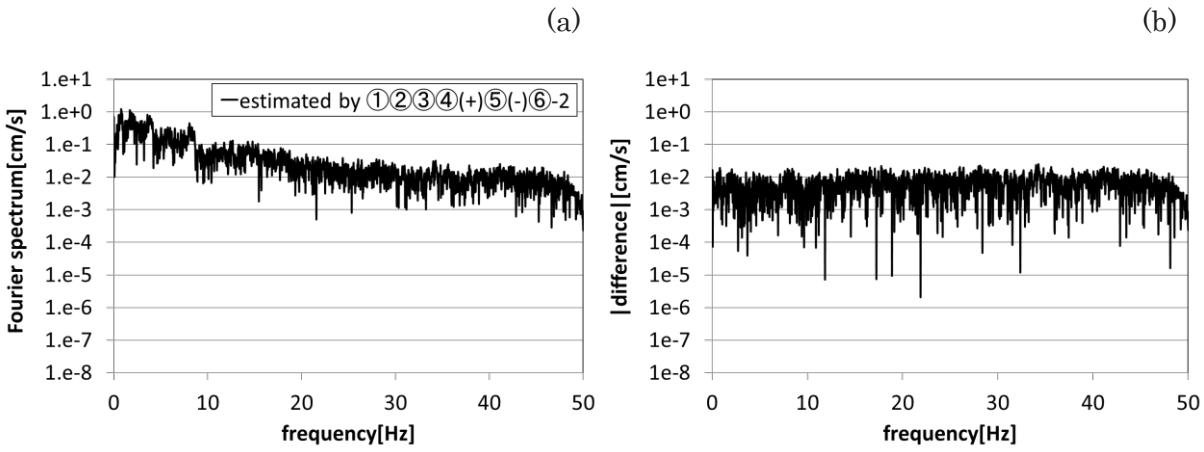

Fig. 31 Fourier spectrum of the estimated acceleration by applying $F_1(f)$, $F_2(f)$, $F_3(f)$, $F_{4+}(t)$, $F_{5-}(t)$ and the LSAR model (estimated by ①②③④(+)⑤(-)⑥-2) (a), and the absolute value of difference of Fourier spectrums before and after applying the LSAR model (b).

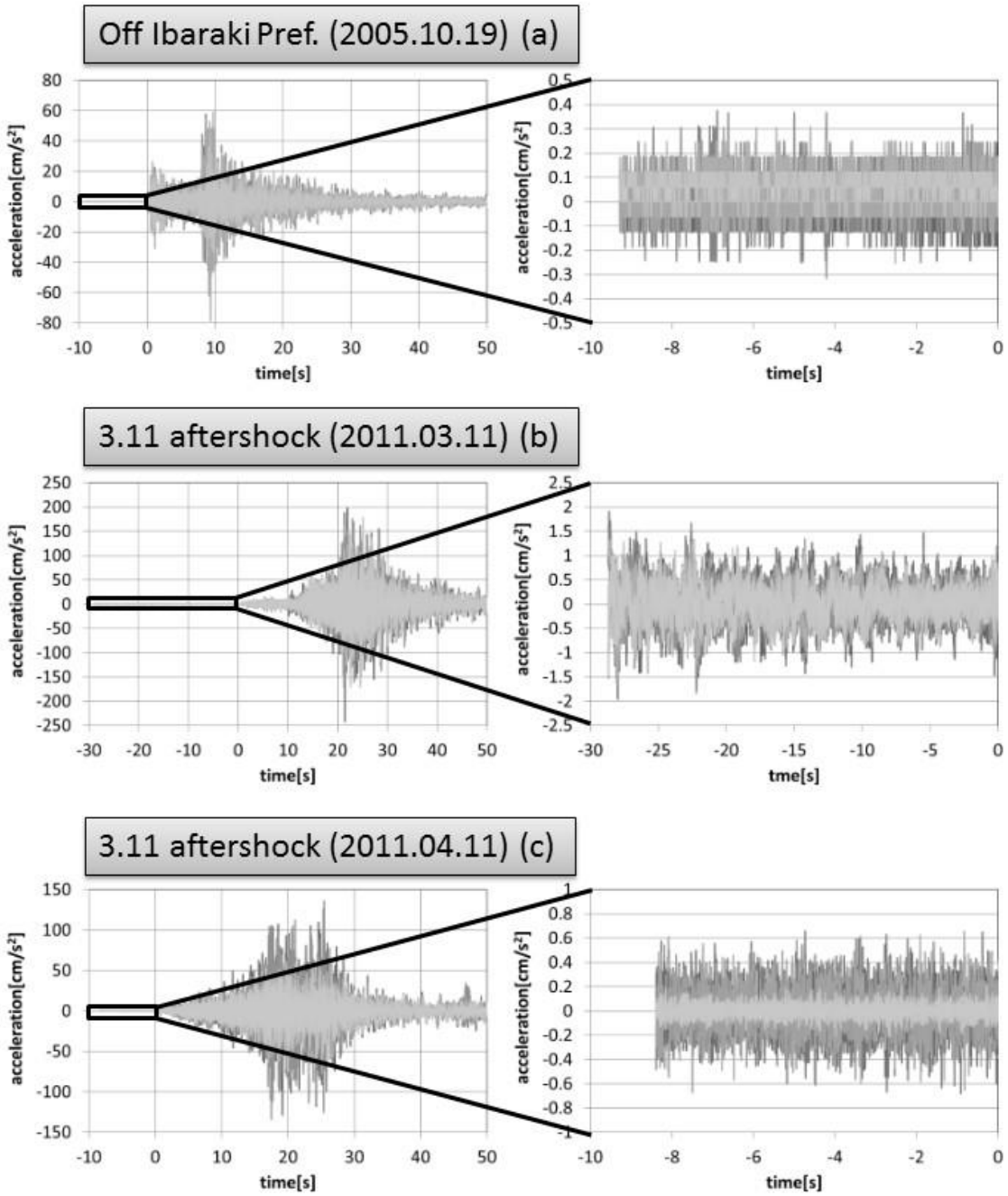

Fig. 32 Time series of observed accelerations for seismic motions No. 4 (a), 6 (b) and 7 (c).

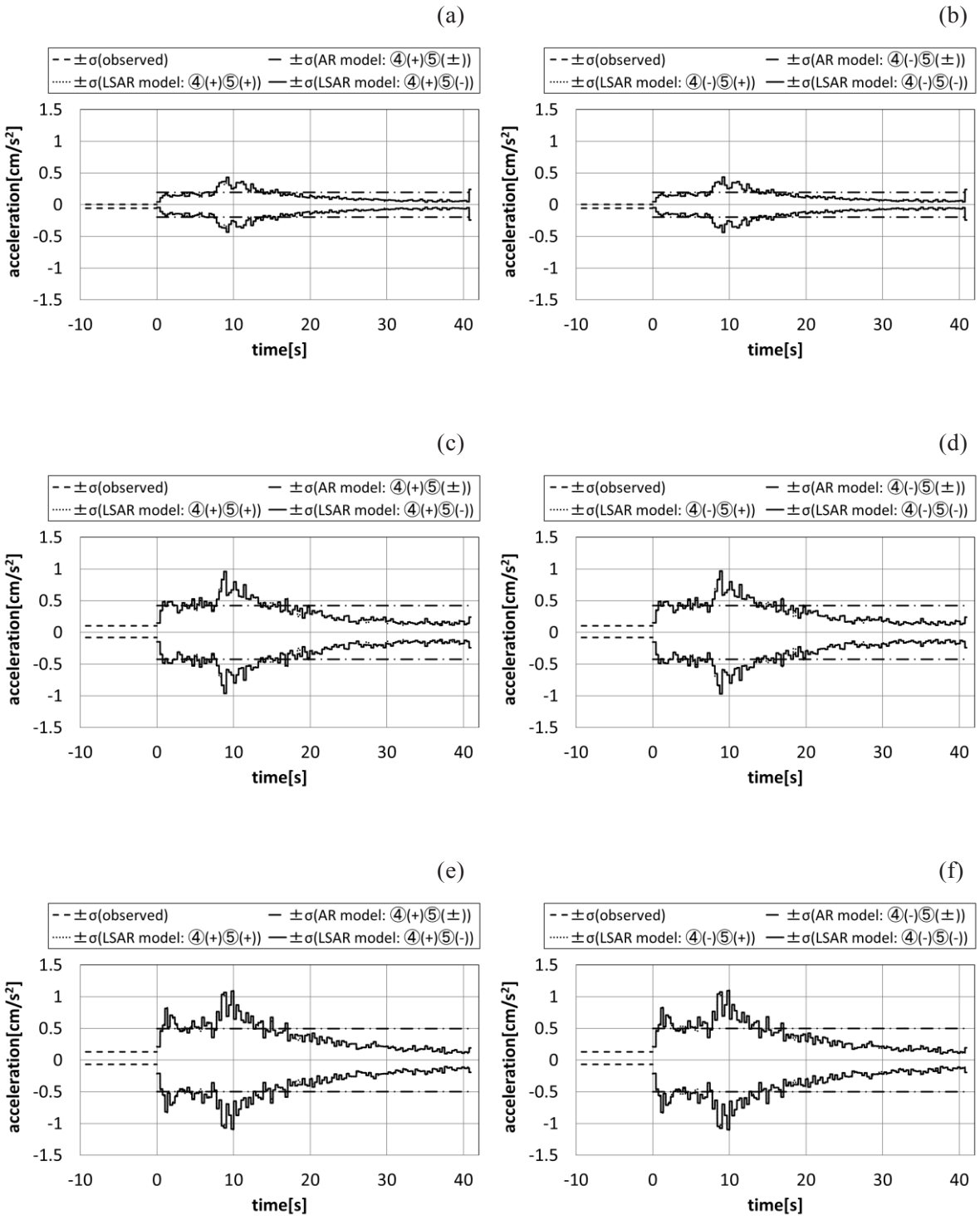

Fig. 33 Time series of the standard deviation of disturbance acceleration (for $t \le 0$), white noise in the AR model (for $t \ge 0$) and white noise in the LSAR model (for $t \ge 0$) at the center in B3 floor for $F_{4+}(t)$ and $F_{5\pm}(t)$ (a) and for $F_{4-}(t)$ and $F_{5\pm}(t)$ (b), south side in the 1st floor for $F_{4+}(t)$ and $F_{5\pm}(t)$ (c) and for $F_{4-}(t)$ and $F_{5\pm}(t)$ (d), and south side in the 2nd floor for $F_{4+}(t)$ and $F_{5\pm}(t)$ (e) and for $F_{4-}(t)$ and $F_{5\pm}(t)$ (f) for the seismic motion of No. 4.

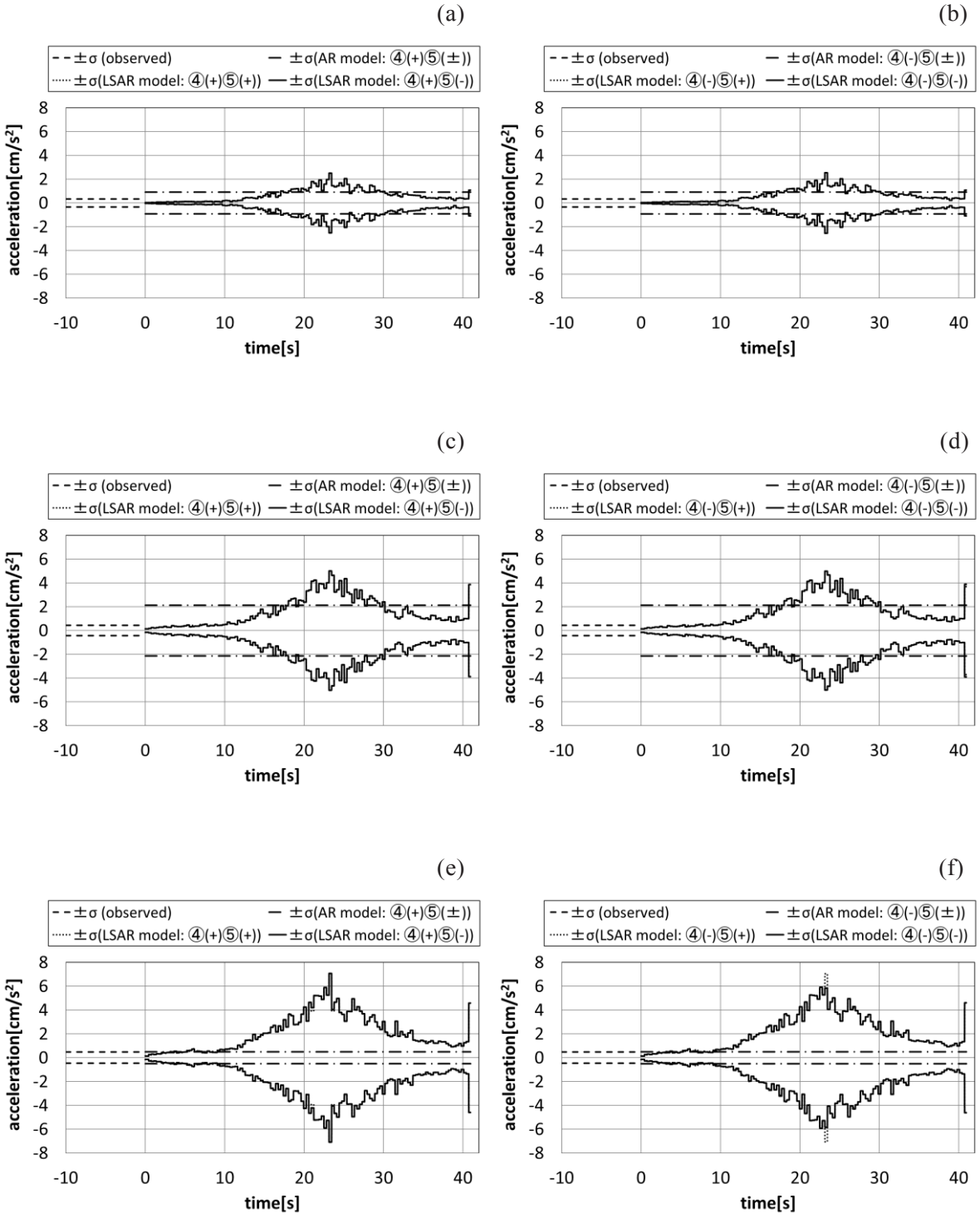

Fig. 34 Time series of the standard deviation of disturbance acceleration (for $t \le 0$), white noise in the AR model (for $t \ge 0$) and white noise in the LSAR model (for $t \ge 0$) at the center in B3 floor for $F_{4+}(t)$ and $F_{5\pm}(t)$ (a) and for $F_{4-}(t)$ and $F_{5\pm}(t)$ (b), south side in the 1st floor for $F_{4+}(t)$ and $F_{5\pm}(t)$ (c) and for $F_{4-}(t)$ and $F_{5\pm}(t)$ (d), and south side in the 2nd floor for $F_{4+}(t)$ and $F_{5\pm}(t)$ (e) and for $F_{4-}(t)$ and $F_{5\pm}(t)$ (f) for the seismic motion of No. 6.

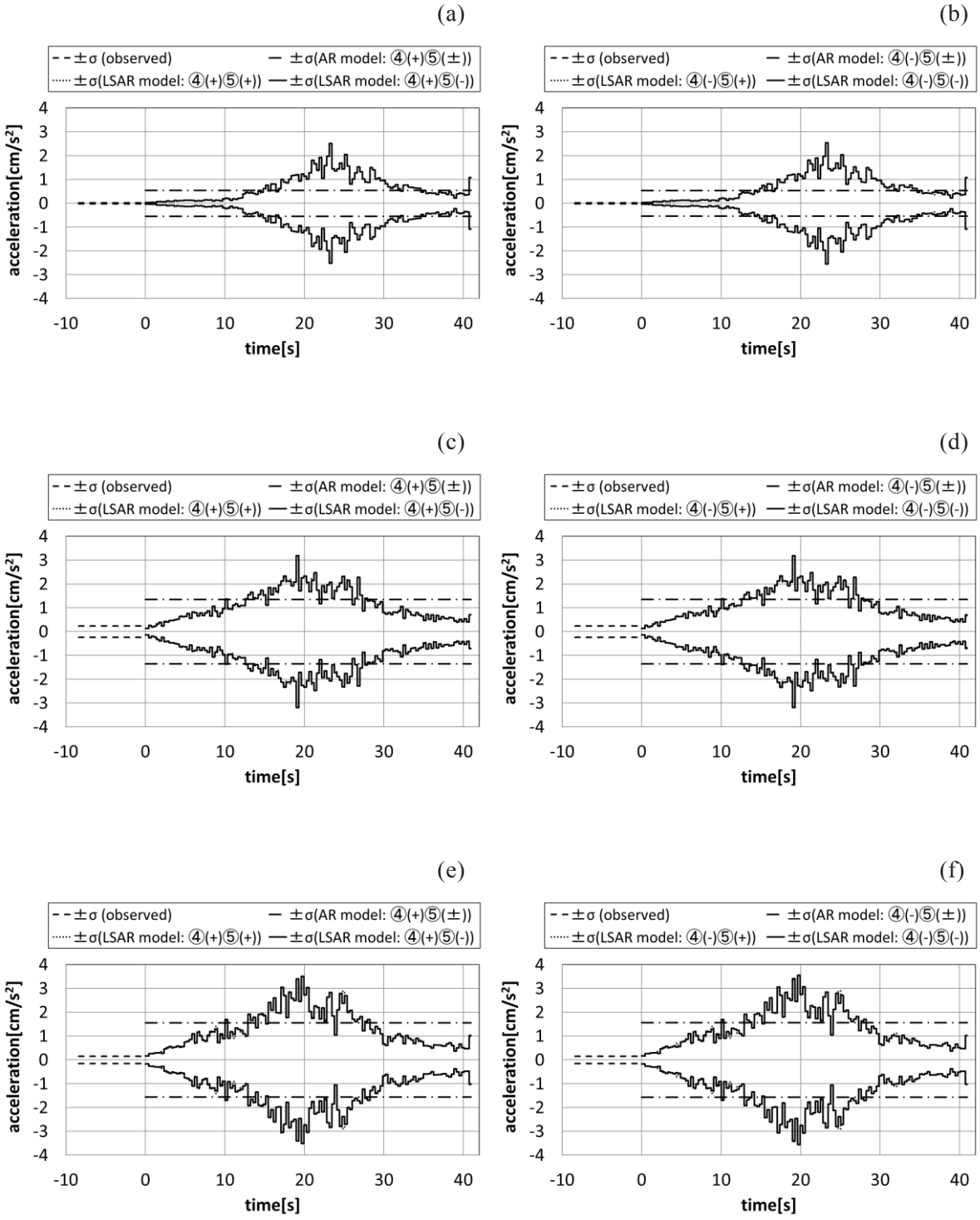

Fig. 35 Time series of the standard deviation of disturbance acceleration (for $t \le 0$), white noise in the AR model (for $t \ge 0$) and white noise in the LSAR model (for $t \ge 0$) at the center in B3 floor for $F_{4+}(t)$ and $F_{5\pm}(t)$ (a) and for $F_{4-}(t)$ and $F_{5\pm}(t)$ (b), south side in the 1st floor for $F_{4+}(t)$ and $F_{5\pm}(t)$ (c) and for $F_{4-}(t)$ and $F_{5\pm}(t)$ (d), and south side in the 2nd floor for $F_{4+}(t)$ and $F_{5\pm}(t)$ (e) and for $F_{4-}(t)$ and $F_{5\pm}(t)$ (f) for the seismic motion of No. 7.

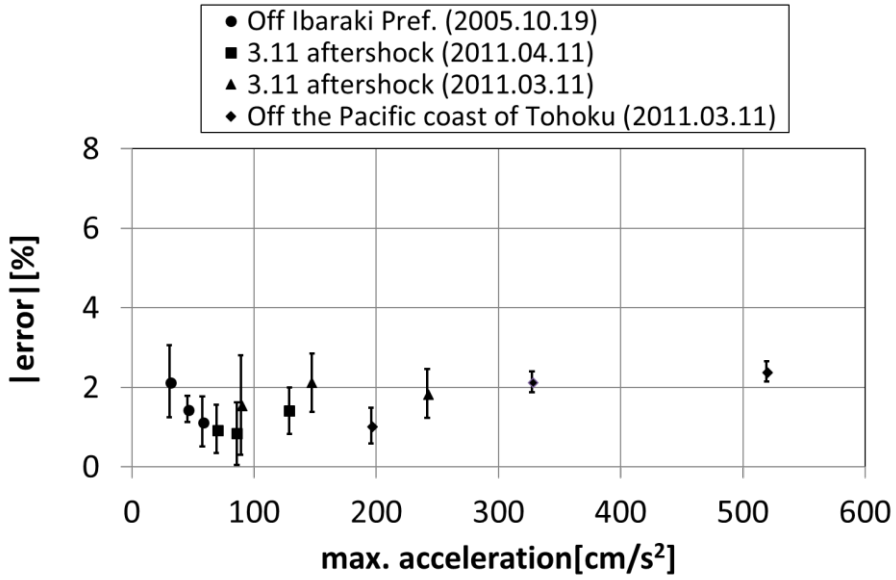

Fig. 36 Maximum accelerations vs. absolute values of error after applying $F_1(f)$, $F_2(f)$, $F_3(f)$, $F_{4\pm}(t)$ and $F_{5\pm}(t)$ for four seismic motions No. 4, 5, 6 and 7.

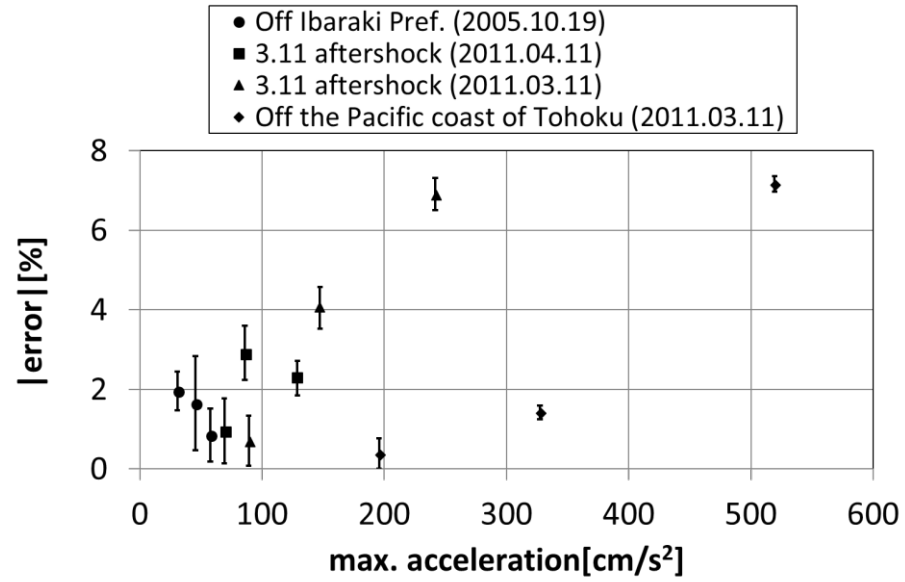

Fig. 37 Maximum accelerations vs. absolute values of error after applying $F_1(f)$, $F_2(f)$, $F_3(f)$, $F_{4\pm}(t)$, $F_{5\pm}(t)$ and the AR model for four seismic motions No. 4, 5, 6 and 7.

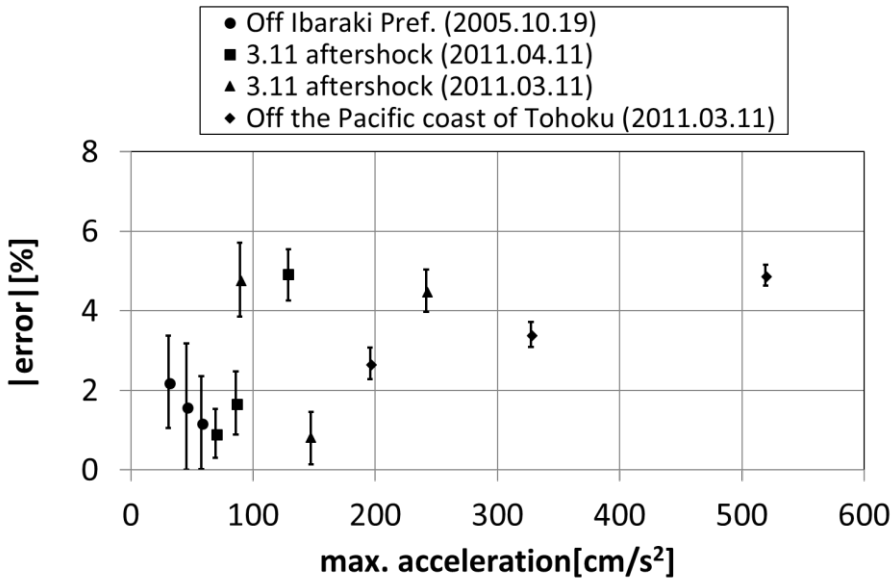

Fig. 38 Maximum accelerations vs. absolute values of error after applying $F_1(f)$, $F_2(f)$, $F_3(f)$, $F_{4\pm}(t)$, $F_{5\pm}(t)$ and the LSAR model for four seismic motions No. 4, 5, 6 and 7.

This is a blank page.

国際単位系（SI）

表１．SI 基本単位

基本量	SI 基本単位	
	名称	記号
長さ	メートル	m
質量	キログラム	kg
時間	秒	s
電流	アンペア	A
熱力学温度	ケルビン	K
物質量	モル	mol
光度	カンデラ	cd

表２．基本単位を用いて表されるSI組立単位の例

組立量	SI 組立単位	
	名称	記号
面積	平方メートル	m^2
体積	立方メートル	m^3
速さ，速度	メートル毎秒	m/s
加速度	メートル毎秒毎秒	m/s^2
波数	毎メートル	m^{-1}
密度，質量密度	キログラム毎立方メートル	kg/m^3
面積密度	キログラム毎平方メートル	kg/m^2
比体積	立方メートル毎キログラム	m^3/kg
電流密度	アンペア毎平方メートル	A/m^2
磁界の強さ	アンペア毎メートル	A/m
量濃度(a)，濃度	モル毎立方メートル	mol/m^3
質量濃度	キログラム毎立方メートル	kg/m^3
輝度	カンデラ毎平方メートル	cd/m^2
屈折率(b)	（数字の） 1	1
比透磁率(b)	（数字の） 1	1

(a) 量濃度（amount concentration）は臨床化学の分野では物質濃度（substance concentration）ともよばれる。
(b) これらは無次元量あるいは次元１をもつ量であるが、そのことを表す単位記号である数字の１は通常は表記しない。

表３．固有の名称と記号で表されるSI組立単位

組立量	SI 組立単位			
	名称	記号	他のSI単位による表し方	SI基本単位による表し方
平面角	ラジアン(b)	rad	1 (b)	m/m
立体角	ステラジアン(b)	sr(c)	1 (b)	m^2/m^2
周波数	ヘルツ(d)	Hz		s^{-1}
力	ニュートン	N		m kg s^{-2}
圧力，応力	パスカル	Pa	N/m^2	m^{-1} kg s^{-2}
エネルギー，仕事，熱量	ジュール	J	N m	m^2 kg s^{-2}
仕事率，工率，放射束	ワット	W	J/s	m^2 kg s^{-3}
電荷，電気量	クーロン	C		s A
電位差（電圧），起電力	ボルト	V	W/A	m^2 kg s^{-3} A^{-1}
静電容量	ファラド	F	C/V	m^{-2} kg^{-1} s^4 A^2
電気抵抗	オーム	Ω	V/A	m^2 kg s^{-3} A^{-2}
コンダクタンス	ジーメンス	S	A/V	m^{-2} kg^{-1} s^3 A^2
磁束	ウエーバ	Wb	Vs	m^2 kg s^{-2} A^{-1}
磁束密度	テスラ	T	Wb/m^2	kg s^{-2} A^{-1}
インダクタンス	ヘンリー	H	Wb/A	m^2 kg s^{-2} A^{-2}
セルシウス温度	セルシウス度(e)	℃		K
光束	ルーメン	lm	cd sr(c)	cd
照度	ルクス	lx	lm/m^2	m^{-2} cd
放射性核種の放射能(f)	ベクレル(d)	Bq		s^{-1}
吸収線量，比エネルギー分与，カーマ	グレイ	Gy	J/kg	m^2 s^{-2}
線量当量，周辺線量当量，方向性線量当量，個人線量当量	シーベルト(g)	Sv	J/kg	m^2 s^{-2}
酸素活性	カタール	kat		s^{-1} mol

(a)SI接頭語は固有の名称と記号を持つ組立単位と組み合わせても使用できる。しかし接頭語を付した単位はもはやコヒーレントではない。
(b)ラジアンとステラジアンは数字の１に対する単位の特別な名称で、量についての情報をつたえるために使われる。実際には、使用する時には記号radおよびsrが用いられるが、習慣として組立単位としての記号である数字の１は明示されない。
(c)測光学ではステラジアンという名称と記号srを単位の表し方の中に、そのまま維持している。
(d)ヘルツは周期現象についてのみ、ベクレルは放射性核種の統計的過程についてのみ使用される。
(e)セルシウス度はケルビンの特別な名称で、セルシウス温度を表すために使用される。セルシウス度とケルビンの単位の大きさは同一である。したがって、温度差や温度間隔を表す数値はどちらの単位で表しても同じである。
(f)放射性核種の放射能（activity referred to a radionuclide）は、しばしば誤った用語で"radioactivity"と記される。
(g)単位シーベルト（PV,2002,70,205）についてはCIPM勧告2（CI-2002）を参照。

表４．単位の中に固有の名称と記号を含むSI組立単位の例

組立量	SI 組立単位		
	名称	記号	SI 基本単位による表し方
粘度	パスカル秒	Pa s	m^{-1} kg s^{-1}
力のモーメント	ニュートンメートル	N m	m^2 kg s^{-2}
表面張力	ニュートン毎メートル	N/m	kg s^{-2}
角速度	ラジアン毎秒	rad/s	m m^{-1} s^{-1}=s^{-1}
角加速度	ラジアン毎秒毎秒	rad/s^2	m m^{-1} s^{-2}=s^{-2}
熱流密度，放射照度	ワット毎平方メートル	W/m^2	kg s^{-3}
熱容量，エントロピー	ジュール毎ケルビン	J/K	m^2 kg s^{-2} K^{-1}
比熱容量，比エントロピー	ジュール毎キログラム毎ケルビン	J/(kg K)	m^2 s^{-2} K^{-1}
比エネルギー	ジュール毎キログラム	J/kg	m^2 s^{-2}
熱伝導率	ワット毎メートル毎ケルビン	W/(m K)	m kg s^{-3} K^{-1}
体積エネルギー	ジュール毎立方メートル	J/m^3	m^{-1} kg s^{-2}
電界の強さ	ボルト毎メートル	V/m	m kg s^{-3} A^{-1}
電荷密度	クーロン毎立方メートル	C/m^3	m^{-3} s A
表面電荷	クーロン毎平方メートル	C/m^2	m^{-2} s A
電束密度，電気変位	クーロン毎平方メートル	C/m^2	m^{-2} s A
誘電率	ファラド毎メートル	F/m	m^{-3} kg^{-1} s^4 A^2
透磁率	ヘンリー毎メートル	H/m	m kg s^{-2} A^{-2}
モルエネルギー	ジュール毎モル	J/mol	m^2 kg s^{-2} mol^{-1}
モルエントロピー，モル熱容量	ジュール毎モル毎ケルビン	J/(mol K)	m^2 kg s^{-2} K^{-1} mol^{-1}
照射線量（X線及びγ線）	クーロン毎キログラム	C/kg	kg^{-1} s A
吸収線量率	グレイ毎秒	Gy/s	m^2 s^{-3}
放射強度	ワット毎ステラジアン	W/sr	m^4 m^{-2} kg s^{-3}=m^2 kg s^{-3}
放射輝度	ワット毎平方メートル毎ステラジアン	$W/(m^2$ sr)	m^2 m^{-2} kg s^{-3}=kg s^{-3}
酵素活性濃度	カタール毎立方メートル	kat/m^3	m^{-3} s^{-1} mol

表５．SI 接頭語

乗数	名称	記号	乗数	名称	記号
10^{24}	ヨタ	Y	10^{-1}	デシ	d
10^{21}	ゼタ	Z	10^{-2}	センチ	c
10^{18}	エクサ	E	10^{-3}	ミリ	m
10^{15}	ペタ	P	10^{-6}	マイクロ	μ
10^{12}	テラ	T	10^{-9}	ナノ	n
10^{9}	ギガ	G	10^{-12}	ピコ	p
10^{6}	メガ	M	10^{-15}	フェムト	f
10^{3}	キロ	k	10^{-18}	アト	a
10^{2}	ヘクト	h	10^{-21}	ゼプト	z
10^{1}	デカ	da	10^{-24}	ヨクト	y

表６．SIに属さないが、SIと併用される単位

名称	記号	SI 単位による値
分	min	1 min=60 s
時	h	1 h =60 min=3600 s
日	d	1 d=24 h=86 400 s
度	°	1°=(π/180) rad
分	’	1’=(1/60)°=(π/10 800) rad
秒	”	1”=(1/60)’=(π/648 000) rad
ヘクタール	ha	1 ha=1 hm^2=10^4m^2
リットル	L, l	1 L=1 l=1 dm^3=10^3cm^3=$10^{-3}m^3$
トン	t	1 t=10^3 kg

表７．SIに属さないが、SIと併用される単位で、SI単位で表される数値が実験的に得られるもの

名称	記号	SI 単位で表される数値
電子ボルト	eV	1 eV=1.602 176 53(14)×10^{-19}J
ダルトン	Da	1 Da=1.660 538 86(28)×10^{-27}kg
統一原子質量単位	u	1 u=1 Da
天文単位	ua	1 ua=1.495 978 706 91(6)×10^{11}m

表８．SIに属さないが、SIと併用されるその他の単位

名称	記号	SI 単位で表される数値
バール	bar	1 bar=0.1MPa=100 kPa=10^5Pa
水銀柱ミリメートル	mmHg	1 mmHg≈133.322Pa
オングストローム	Å	1 Å=0.1nm=100pm=10^{-10}m
海里	M	1 M=1852m
バーン	b	1 b=100fm^2=(10^{-12}cm)^2=$10^{-28}m^2$
ノット	kn	1 kn=(1852/3600)m/s
ネーパ	Np	SI単位との数値的な関係は、対数量の定義に依存。
ベル	B	
デシベル	dB	

表９．固有の名称をもつCGS組立単位

名称	記号	SI 単位で表される数値
エルグ	erg	1 erg=10^{-7} J
ダイン	dyn	1 dyn=10^{-5}N
ポアズ	P	1 P=1 dyn s cm^{-2}=0.1Pa s
ストークス	St	1 St =1cm^2 s^{-1}=$10^{-4}m^2$ s^{-1}
スチルブ	sb	1 sb =1cd cm^{-2}=10^4cd m^{-2}
フォト	ph	1 ph=1cd sr cm^{-2} =10^4lx
ガル	Gal	1 Gal =1cm s^{-2}=$10^{-2}ms^{-2}$
マクスウエル	Mx	1 Mx = 1G cm^2=10^{-8}Wb
ガウス	G	1 G =1Mx cm^{-2} =10^{-4}T
エルステッド(a)	Oe	1 Oe ≙ (10^3/4π)A m^{-1}

(a) ３元系のCGS単位系とSIでは直接比較できないため、等号「 ≙ 」は対応関係を示すものである。

表10．SIに属さないその他の単位の例

名称	記号	SI 単位で表される数値
キュリー	Ci	1 Ci=3.7×10^{10}Bq
レントゲン	R	1 R = 2.58×10^{-4}C/kg
ラド	rad	1 rad=1cGy=10^{-2}Gy
レム	rem	1 rem=1 cSv=10^{-2}Sv
ガンマ	γ	1 γ=1 nT=10^{-9}T
フェルミ		1 フェルミ=1 fm=10^{-15}m
メートル系カラット		1 メートル系カラット= 0.2 g = 2×10^{-4}kg
トル	Torr	1 Torr = (101 325/760) Pa
標準大気圧	atm	1 atm = 101 325 Pa
カロリー	cal	1 cal=4.1858J（「15℃」カロリー），4.1868J（「IT」カロリー），4.184J（「熱化学」カロリー）
ミクロン	μ	1 μ =1μm=10^{-6}m

（第8版，2006年）